Crustal partial melting on Vesta: evidence from highly metamorphosed eucrites

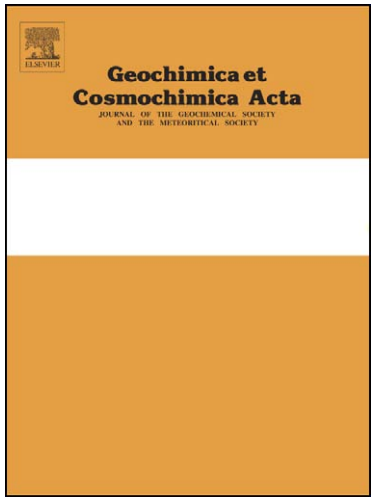

Crustal partial melting on Vesta: Evidence from highly metamorphosed eucrites

A. Yamaguchi, J.A. Barrat, R.C. Greenwood, N. Shirai, C. Okamoto, T. Setoyanagi, M. Ebihara, I.A. Franchi, M. Bohn

PII: S0016-7037(09)00504-3
DOI: 10.1016/j.gca.2009.07.037
Reference: GCA 6404

To appear in: *Geochimica et Cosmochimica Acta*

Received Date: 30 January 2009
Accepted Date: 27 July 2009

Please cite this article as: Yamaguchi, A., Barrat, J.A., Greenwood, R.C., Shirai, N., Okamoto, C., Setoyanagi, T., Ebihara, M., Franchi, I.A., Bohn, M., Crustal partial melting on Vesta: Evidence from highly metamorphosed eucrites, *Geochimica et Cosmochimica Acta* (2009), doi: 10.1016/j.gca.2009.07.037

Crustal partial melting on Vesta:

Evidence from highly metamorphosed eucrites

A. Yamaguchi[1,2,3], J.A. Barrat[3], R. C. Greenwood[4], N. Shirai[5,6], C. Okamoto[5,7], T. Setoyanagi[5], M. Ebihara[5], I.A. Franchi[4] and M. Bohn[3]

[1]*National Institute of Polar Research, Tachikawa, Tokyo 190-8518, Japan (yamaguch@nipr.ac.jp)*

[2]*Department of Polar Science, School of Multidisciplinary Science, Graduate University for Advanced Sciences, Tokyo 173-8515, Japan*

[3]*Université Européenne de Bretagne, U.B.O.-I.U.E.M., CNRS UMR 6538, Place Nicolas Copernic, 29280 Plouzané Cedex, France*

[4]*PSSRI, The Open University, Walton Hall, Milton Keynes MK7 6AA, United Kingdom*

[5]*Department of Chemistry, Tokyo Metropolitan University, Hachioji, Tokyo 192-0397, Japan*

[6]*National High Magnetic Field Laboratory and Department of Geological Sciences, Florida State University, 1800 E. Paul Dirac Drive, Tallahassee, FL 32310, USA*

[7]*Graduate School of Environmental Studies, Nagoya University, Furo-cho, Nagoya 464-8601, Japan*

This is a revised version of the manuscript submitted on January 30, 2009

Abstract

We have performed a mineralogical and geochemical study of eight metamorphosed basaltic eucrites. These are classified into granulitic eucrites and type 4-7 eucrites on the basis of their textures and pyroxene mineralogy, and display mineralogical evidence for high temperature metamorphism, including partial melting. In particular, rare earth element (REE) patterns of a number of the eucrites studied show varying degrees of light REE depletion due to partial melting, with subsequent melt extraction. A simple correlation between metamorphic grade, as deduced from pyroxene mineralogy, and the degree of light REE depletion was not detected. This can be explained by the fact that homogenization, exsolution and inversion of pigeonite would have required prolonged heating at moderate temperatures (~800-1000 °C), whereas partial melting would have taken place over a short time interval where temperatures exceeded that of the solidus. The eucrites studied therefore record a two stage thermal regime consisting of short, high temperature reheating events superimposed on long duration global crustal metamorphism. The short reheating events may have been caused by impact events and/or intrusions of hot magmas. The results of this study demonstrate that the thermal history of eucritic crust was more complex than can be explained by a simple burial model alone. In particular, the origin of Stannern trend eucrites requires contamination of Main-Group magmas by partial melts extracted from residual eucrites.

1. Introduction

Howardites, eucrites, and diogenites (HED-meteorites) represent the largest group of achondrites and are generally regarded as being samples from the crust of the asteroid 4-Vesta (e.g., McCord, 1970; Binzel and Hsu, 1993). Eucrites are pigeonite-plagioclase basalts and gabbros, diogenites are orthopyroxenites, howardites are mechanical mixtures of impact-derived material from eucrites and diogenites. Howardites may also contain a minor xenolithic component. HED meteorites preserve a uniquely detailed record of igneous processes on an early formed basaltic asteroid, with the start of magmatic activity on their parent body being dated to within 3 Ma of solar system formation (e.g., Nyquist et al., 1986; Bizzaro et al., 2005, Misawa et al., 2006). Although a range of models have been proposed for the origin of HED meteorites, large scale melting, leading to the development of a magma ocean is generally accepted as a plausible means of explaining their geochemical and oxygen isotopic characteristics (e.g., Righter and Drake, 1996; 1997; Barrat et al., 2007; Greenwood et al., 2005). After extensive differentiation, the crust of the HED parent body may have had a layered structure, consisting of an outer eucritic crust, underlain by diogenitic-rich material, enclosing an ultramafic mantle and metallic core (e.g., Takeda, 1979; Righter and Drake, 1997; Barrat, 2004).

Unbrecciated eucrites, and eucritic clasts in HED breccias, are classified into two groups; (i) basaltic (noncumulate) eucrites and (ii) cumulate eucrites, on the basis of their texture and bulk chemical composition (e.g., Mittlefehldt et al., 1998). Basaltic eucrites cooled quickly, either as lavas or shallow intrusions. Pyroxene textures and mineralogy (e.g., Takeda, 1997) indicate that cumulate eucrites crystallized more slowly, probably within lower crustal magma chambers. The magmas that produced the cumulate eucrites were probably similar to those from which the basaltic eucrites formed, and would have comprised cumulate crystals of pyroxene and/or plagioclase with variable amounts of trapped liquid (Treiman, 1997; Barrat, 2003).

Basaltic eucrites are subdivided into two chemical groups: (i) Main-Group – Nuevo Laredo trend eucrites, and (ii) Stannern trend eucrites (e.g., Stolper, 1977; Warren and Jerde, 1987). Stannern trend eucrites are compositionally close to those of the Main-Group with respect to major elements, but are significantly richer in incompatible elements. Main-Group–Nuevo Laredo trend eucrites display wide variations in Mg' (= molar Mg/(Mg+Fe)) with only moderate variations in incompatible elements and are believed to represent a fractional crystallization trend. The Stannern trend eucrites have more limited Mg' variation, but show significant incompatible element variation. The occurrence of these two chemical groups is difficult to explain using models that invoke only progressive crystallization of a magma ocean (e.g., Barrat et al., 2000; Mittlefehldt and Lindstrom, 2003).

Almost all basaltic eucrites experienced varying degrees of metamorphism and have been classified into seven types (type 1-7) on the basis of their textures and mineralogy (Takeda and Graham, 1991; Yamaguchi et al, 1996). The majority of basaltic eucrites were metamorphosed at temperatures ranging from 700-1000 °C (Takeda and Graham, 1991; Yamaguchi et al., 1996; Mayne et al. 2009), although some experienced conditions close to, or exceeding the solidus (~1060°C) (Floss et al., 2000; Yamaguchi et al., 2001). To explain this thermal history Yamaguchi et al. (1996, 1997b) proposed that eucritic crust developed through rapid accumulation of lava eruptions resulting in burial and metamorphism by internal heat. This model predicts that the earliest eucritic flows should be the most metamorphosed because they were buried towards the base of the crust, whereas the youngest eucrites are likely to be the least metamorphosed because they remained essentially unburied. Thus, the degree of metamorphism may be correlated to the timing of eruption and intrusion.

The crust of the HED parent body was extensively reworked by impact events and as a consequence almost all eucrites show evidence of brecciation, and sometimes impact melting and recrystallization (Yamaguchi et al., 1994; Metzler et al., 1995; Yamaguchi et al., 1996; Barrat et al., 2003). These impact events occurred before, during, and after thermal

metamorphism (Metzler et al., 1995; Yamaguchi et al., 1996). The shock and thermal histories recorded by eucrites demonstrate that the crust of the HED parent body evolved through repeated lava eruptions, magma intrusion and subsequent metamorphism. In addition, impact events and igneous activity may have occurred simultaneously resulting in destruction and excavation of magma, which was then mixed with already crystallized rock (Scott et al., 1989).

Recently, attempts have been made to correlate petrologic and chemical features in order to understand the processes involved in the formation of eucritic crust. Warren and Kallemeyn (2001) suggested that the metamorphic grade and bulk incompatible element abundance are roughly correlated. The majority of weakly metamorphosed eucrites (type 1-4) are generally enriched in incompatible elements (e.g., Bouvante, Stannern), whereas most Main-Group trend eucrites are type 5 to 7. This metamorphism-composition correlation would appear to support the magma ocean model because incompatible element abundances in melts increase as fractional crystallization proceeds. However, the model of Warren and Kallemeyn (2001) does not adequately account for the origin of Stannern trend eucrites. In addition, because eucrites experienced complex thermal histories, the degree of metamorphism is probably not a simple linear trend of progressive mineralogical changes in response to increasing temperature (Schwartz and McCallum, 2005).

Barrat et al. (2007) have put forward a model involving contamination of normal Main-Group eucrites by crustal partial melts to explain both the thermal history and chemical characteristics of Stannern trend eucrites. This model is compatible with the view that the crust of the parent body formed chiefly through rapid accumulation of lava flows (Yamaguchi et al., 1996; 1997b). Thus, the partially melted eucrites would have been deeply buried and hence highly metamorphosed. On the basis of ion microprobe analyses and mineralogical data, Floss et al. (2000) and Yamaguchi et al. (2001) suggested that the highly metamorphosed eucrites, Elephant Moraine (EET) 90020 and Yamato (Y) 86763 experienced

partial melting. Preliminary studies indicated that the metamorphosed eucrites, Asuka (A)-87272 and Dar al Gani (DaG) 945 have light REE depleted patterns which probably result from partial melting (Yamaguchi et al., 2007). Bermingham et al. (2008) reported that Pecora Escarpment (PCA) 82502, PCA 91078 and Meteorite Hills (MET) 01081 have light REE depleted patterns, although they suggested that this indicated a derivation from a plagioclase-rich source.

Here, we present the results of a petrologic and geochemical study of eight metamorphosed eucrites, which are likely to have been derived from the deep crust of the HED parent body. The aim of the study was to compare thermal histories and chemical data in order to explain the main processes involved in eucritic crust formation. We will show that at least some metamorphosed basaltic eucrites could be residues after extraction of partial melts. We also performed oxygen isotope analysis on all the investigated samples to ensure that they were isotopically normal members of the HED suite, and hence from the same parent body as regular eucrites.

2. Samples and Analytical techniques

Samples of five Asuka eucrites (A-87272, -880702, -880761, -881388, and -881467) were supplied by the National Institute of Polar Research (NIPR), Tokyo. Chips of desert meteorites (Agoult, DaG 945 and Northwest Africa (NWA) 2362) were obtained from meteorite dealers.

A-87272 is a large, coarse-grained eucrite (5.7 kg) (Yanai and Kojima, 1995). We obtained two portions of A-87272 located ~20 cm apart. One portion was a subsample of the powder previously prepared for wet chemical analysis (3.540 g) (Yanai and Kojima, 1995), the other (2.459 g) was taken from the opposite side of the main mass. A subsample of powder was prepared from the second portion for chemical analysis. A new polished thin section (PTS) of A-87272 was prepared and its texture compared to the sections used in

earlier studies (Yamaguchi et al., 1997; Takeda et al., 1997). A-880702 (0.205 g), A-880761 (0.210 g) and A-881388 (0.227 g) were supplied as chips. A-881467 (0.327 g) was a subsample of powder previously prepared for wet chemical analysis (1.163 g).

PTSs of these eucrites were examined using an optical microscope, scanning electron microscope (SEM) (JSM5900LV) equipped with an energy dispersive spectrometer (EDS) (Oxford Link-ISIS), and electron microprobe analyzer (EPMA) (JXA8200) at NIPR. Mineral modes were determined by X-ray mapping. Silica polymorphs were identified using a laser micro Raman spectrometer (JASCO NRS-1000) at NIPR.

Bulk chemical analysis was performed both in Brest and Tokyo. In Brest, large fragments (typically 1-2 g) were finely ground using a boron carbide pestle and mortar. Major elements were determined at the Université de Bretagne Occidentale in Brest, by ICP-AES (inductively coupled plasma-atomic emission spectrometry) using the procedure described by Cotten et al. (1995). The accuracy of this system is better than 5 % and the reproducibility better than 3 %. Trace element concentrations were measured at the Institut Universitaire Europeen de la Mer (IUEM), Plouzané, by ICP-MS (inductively coupled plasma-mass spectrometry) using a Thermo Element 2 spectrometer (Barrat et al., 2007). Based on standard measurements and sample duplicates trace element concentration reproducibility is generally better than 5 %.

In Tokyo, major, minor and trace element abundances for seven eucrites (A-87272, A-881467, A-880702, A-881388, A-880761, DaG 946 and NWA 2362) were determined non-destructively using three nuclear analytical methods: prompt gamma-ray analysis (PGA), instrumental neutron activation analysis (INAA) and instrumental photon activation analysis (IPAA). Powder samples weighing 100-200 mg were first analyzed by PGA, subsequently INAA and IPAA were performed using subsamples of the powders used for PGA. The accuracy was monitored by analyzing the Allende meteorite powder prepared by E. Jarosewich at the Smithsonian Institution and was found to be better than 5% for most

elements except Sr (8%), Zr (7%), La (8%), Sm (9%), Eu (16%), Yb (25%) and Lu (13%). The precision was also determined by replicate analysis of the Allende powder and confirmed to be within 10% for most elements with the exception of K (14%), Zr (12%), Eu (22%), Yb (35%) and Lu (20%). The precision for PGA, INAA and IPAA is roughly correlated with counting statistics in gamma-ray spectrometry. Procedures for these analytical methods have been described by Latif et al. (1999) for PGA, Shirai and Ebihara (2004) for INAA and Ebihara et al. (2000) for IPAA. Among the seven eucrites analyzed by nuclear analytical methods described above, five eucrites (A-87272, A-882467, A-880702, A-881388 and A-880761) were analyzed for REE, Th and U by ICP-MS using a VG-Plasma Quad III spectrometer. The accuracy is better than 5% for all elements and the precision is within 4% for most elements, with the exceptions of Th (8%) and U (6%). The ICP-MS procedures used are essentially the same as those described by Shinotsuka et al. (1996).

A-87272, DaG 945 and NWA 2362 were analyzed both in Brest and Tokyo. The common homogenized powders prepared in Brest were shared by the two groups. The analytical results from Brest and Tokyo are compared in Table 3. Twenty two elements were eventually determined in duplicate. The two data sets show reasonable agreement, with the exception of a few elements; K values determined in Brest are systematically higher than those measured in Tokyo for the three meteorites, and Zr and Hf data from Brest are lower than those from Tokyo for A-87272. REE, Th and U in A-87272 were determined by ICP-MS both in Brest and Tokyo. Although different portions were analyzed, the agreement between the two sets of analyses was good. These elements, and by inference their host mineral(s), are slightly less abundant in A-87272,140 compared with those in A-87272,25. Major and minor element contents of A-87272 have been analyzed twice in Tokyo using different batches (,140 and ,25), with a four-year interval between each set of analysis. This duplicate data was found to be in very good agreement.

Oxygen isotope analysis was carried out using an infrared laser fluorination system

(Miller et al. 1999). 50-100 mg chips of all eight metamorphosed eucrites investigated in this study were crushed and homogenized and replicate analyses undertaken on ~2 mg subsamples of these powders. To maximize yields and decrease the risk of cross-contamination the powdered samples were fused in vacuum to form a glass bead prior to fluorination. O_2 was liberated by heating the glass beads using an infrared CO_2 laser (10.6 μm) in the presence of 210 torr of BrF_5. After fluorination, the O_2 released was purified by passing it through two cryogenic nitrogen traps and over a bed of heated KBr. O_2 was analyzed using a Micromass Prism III dual inlet mass spectrometer. Published system precision (1) (Miller et al., 1999), based on replicate analyses of international (NBS-28 quartz, UWG-2 garnet) and internal standards, is approximately ±0.04‰ for ^{17}O; ±0.08‰ for ^{18}O; ±0.02‰ for ^{17}O. The quoted precision (1) for the eucrite samples is based on replicate analyses. Oxygen isotope values are reported in standard notation, where ^{18}O has been calculated as: $^{18}O = ((^{18}O/^{16}O_{sample}/^{18}O/^{16}O_{ref})-1) \times 1000$ and similarly for ^{17}O using the $^{17}O/^{16}O$ ratio. ^{17}O has been calculated using the linearized format of Miller (2002): $^{17}O = 1000 \ln (1+(^{17}O/1000)) - 1000 \ln (1+(^{18}O/1000))$ where = 0.5247.

3. Results

3.1. Textures and Mineral Chemistry

The eight eucrites examined in this study range from fine- to coarse-grained, with igneous and/or metamorphic textures and are composed of pyroxene, plagioclase, silica minerals (tridymite and quartz), ilmenite, spinels (chromite, ulvöspinel), Ca-phosphates, troilite, and/or Fe-metal and zircon (Figs. 1-3). (Petrologic and chemical properties of eight eucrites are listed in Table 1).

3.1.1. Granulitic eucrites

Eucrites A-880761, -880702, -881388, -881467 and Agoult show granulitic textures with abundant 120° triple junctions and curved boundaries, indicating strong recrystallization (Fig. 1). They range from unshocked to weakly shocked; pyroxene and plagioclase show sharp optical extinction. The petrology of two eucrites, A-881388 and -881467 has been described by several workers (Yamaguchi et al., 1997a; Takeda et al., 1997; Floss et al., 2000). We have subdivided these granulitic eucrites into two types: A and B on the basis of their textures and pyroxene mineralogy.

Type A granulitic eucrites, A-880702 and A-881467 display large variations in grain size from ~30 μm to 1 mm in size, with relict basaltic textures preserved in places (Figs. 1 and 3). Large grains are typically angular to irregular in shape, while smaller grains tend to be more rounded and granular. Large plagioclase grains often have cloudy cores with clear rims (see below). These large grains are likely to be relict mineral fragments from precursor breccias.

Type B granulitic eucrites, Agoult, A-880761 and A-881388 show finer-grained granulitic textures (Figs. 1 and 3). In A-880761 and A-881388, the grain sizes of pyroxene and plagioclase are more sorted (~100 μm in size). Most portions of Agoult show a fine-grained relict, subophitic texture, composed of granular pyroxene (~100 μm in size) and elongate plagioclase (~50 x 300 μm). In contrast, A-880761 and A-881388 contain only a few large plagioclase laths (~500 μm in size), which could be vestiges of the precursor basalts.

Low-Ca pyroxene and augite in the granulitic eucrites both have homogeneous Mg' (Fig. 4 and Table 2) and closely spaced, fine (~1-2 μm thick) exsolution lamellae. In type B granulitic eucrites, pyroxenes are typically homogeneous low-Ca pyroxene and augite grains, whereas in type A only low-Ca pyroxene is present, with the latter displaying remnant Ca zoning with the density (and thickness) of augite lamellae increasing towards the rim. Augite-rich rims are associated with relict mesostasis. Low-Ca pyroxene in type A granulitic

eucrites has slightly lower Mg'. Clouding in pyroxenes, due to the presence of minute opaques (e.g., ilmenite, chromite) (Harlow and Klimentidis, 1980; Mori and Takeda, 1985), is lacking, except for the large grains in type A granulitic eucrites.

Plagioclase in type A eucrites is slightly less calcic (An_{89-85}) than in type B (An_{91-88}) (Fig. 5 and Table 2). The cores of large plagioclase grains often contain fine inclusions (~2 – 30 μm diameter) consisting of pyroxene and silica minerals. These cloudy cores are enclosed by clear rims (~10-50 μm thick). Relict mesostasis in these granulitic eucrites is locally enriched in tridymite. In A-880702, there are relatively large grains (up to ~500 μm) of tridymite, often in contact with augite. In A-881467, fine-grained tridymite grains are scattered throughout the entire thin section, with discrete areas (~1 mm) that are locally enriched in silica minerals and augite. Spinels are chromite and ulvöspinel, often associated with ilmenite and/or Fe and FeS. These spinels display significant chemical variation and are very enriched in Ti compared to other basaltic eucrites (~Usp_{62-69}), with the highest Ti in A-881388 ($Usp_{68.1}Chm_{38.1}$) (Fig. 6). A-881388 and Agoult contain large opaque grains composed of ilmenite, Ti-chromite, and minor Fe-FeS (Arai et al., 1998; this work). In granulitic eucrites, small grains of Ca-phosphate (<several to 50 μm) occur evenly in the PTSs. In A-881467, fine-grained (<20-30 μm), Ca-phosphate occurs sparsely and evenly, although there are increased concentrations within the areas of relict mesostasis.

3.1.2. A-87272

The textures and mineralogy of A-87272 have been reported by several workers (Yamaguchi et al., 1997a; Takeda et al., 1997; Floss et al., 2000). This eucrite is an unbrecciated, coarse-grained (1-2 mm in size) gabbroic rock (Figs. 2a and 3d). A-87272 is highly shocked, with plagioclase mostly converted to maskelynite. Thin shock veins (several tens of μm thick) were observed in thin section. The new PTS of A-87272 is texturally identical to those previously studied (Takeda et al., 1997; Yamaguchi et al., 1997a), although

the abundance of silica minerals is slightly enriched (6 vol %) compared to these older sections (2.4 vol %) (Yamaguchi et al., 1997a). Relict mesostasis is typically composed of fine-grained quartz grains and large tridymite laths (0.1-0.2 x ~2 mm).

Pyroxenes are low-Ca pyroxene (low-Ca pigeonite) with exsolved augite lamellae. Pigeonite in A-87272 is partially inverted to orthopyroxene. Pyroxene compositions form a single tie line from $Wo_{2.2}En_{36.8}Fs_{61.0}$ to $Wo_{43.9}En_{29.0}Fs_{27.1}$ (Fig. 4). The very low Wo content ($Wo_{2.2}$) of low-Ca pyroxene is consistent with the presence of inverted pigeonites. Many pyroxene grains have augite lamellae with remnant Ca zoning toward the relict mesostasis. Two types of augite lamellae were distinguished; one thick (20-40 μm thick) (001) and the other thin (<1-2 μm thick) (100). The presence of remnant Ca-zoning and inversion texture indicates that A-87272 is a type 7 eucrite (Yamaguchi et al., 1997a). Plagioclase (maskelynite) is very clear under the optical microscope and the cloudy inclusions observed in other eucrites (e.g., DaG 945, see below) are generally lacking. Plagioclase compositions ($An_{92.1-89.2}$) are similar to those in the type B granulitic eucrites. Silica minerals are tridymite and quartz. Tridymite contains significant amounts of impurity elements (K_2O: 0-0.17 wt%; Al_2O_3: 0.10-0.24 wt%; FeO: 0-0.46 wt %). Spinels (chromite and ulvöspinel) show strong enrichment of Ti ($Usp_{5.9}Chm_{75.0}$-$Usp_{60.4}Chm_{33.2}$) (Fig. 6). Ca-phosphate is generally fine-grained (<10 μm) and tends to be associated with the areas of relict mesostasis.

3.1.3. DaG 945.

DaG 945 is a coarse-grained, subophitic eucrite mainly composed of anhedral pyroxene and plagioclase laths (1.7 x 0.6 mm), with some fine-grained portions associated with relict mesostasis (Figs. 2b and 3e). 120º triple junctions and curved boundaries between mineral phases are well developed, indicating that significant recrystallization has taken place. Relict mesostasis, which occurs interstitially between large pyroxene and plagioclase crystals, has a fine-grained (~20-50 μm in size), recrystallized texture, composed of tridymite, quartz,

augite, ilmenite, and spinels.

Pyroxene compositions scatter along $Wo_{4.1}En_{34.3}$ to $Wo_{40.3}En_{27.6}$ on the pyroxene quadrilateral (Fig. 4). The Wo content of DaG 945 pyroxenes is similar to that in the granulitic eucrites. Pyroxene preserves remnant Ca-zoning (i.e., type 4) (Fig. 3e). Most pyroxene grains have a clear appearance, but there are minor zones of clouding. Plagioclase preserves igneous zoning, with compositions varying widely from $An_{91.0}Or_{0.4}$ to $An_{83.3}Or_{0.9}$. Most plagioclase grains have a cloudy appearance near their rims due to the presence of minute crystals (< a few μm) of pyroxene and silica minerals. Silica minerals contain small amounts of K_2O (0.12-0.14 wt%), Al_2O_3 (0.22-0.25 wt%) and FeO (0.08-0.36 wt%). Ca-phosphate grains (<10-30 μm) occur sparsely; with their total abundance being the lowest of any of the eucrites examined in this study.

3.1.4. NWA 2362

NWA 2362 has a medium-grained gabbroic texture and is mainly composed of anhedral pyroxene and elongate plagioclase (~0.3-0.6 mm in size) (Figs. 2c and 3f). This meteorite is slightly shocked: pyroxene and plagioclase have fractures and show mottled extinction. In addition, one half of the thin section studied displayed a well-developed brecciated texture. Relict mesostasis (0.1-0.4 mm in size) is present as large irregular, angular-shaped areas, composed of fine-grained tridymite and quartz with very minute (~ a few μm) grains of troilite.

Low-Ca pyroxene contains both thick (30-40 μm thick) and thin (<1-2 μm thick) augite lamellae. The composition varies from $Wo_{2.7}En_{37.8}Fs_{59.5}$ to $Wo_{44.3}En_{30.2}Fs_{25.6}$ (Fig. 4). The Wo content of low-Ca pyroxene is very low, being similar to that of low-Ca pyroxene in A-87272. However, we could not find inversion textures in NWA 2362 pyroxenes under the optical microscope. Plagioclase preserves original igneous zoning ($An_{91.8}Or_{0.2}$ – $An_{87.4}Or_{0.5}$) (Fig. 5). Silica minerals (tridymite and quartz) contain small amounts of K_2O (0.01-0.08

wt%), Al_2O_3 (0.11-0.69 wt%), and FeO (0.08-0.19 wt%). Chromite has a very low Ti content ($Usp_{3.2\text{-}7.1}Chm_{74.4\text{-}78.0}$) unlike the other eucrites (Fig. 6) (see above). The Ca-phosphate grains (<10-20 μm) occur sparsely; the abundance of Ca-phosphate is very low.

3.2. Major and trace element abundances

Major and trace element compositions of the highly metamorphosed eucrites analyzed during the course of the study are given in Table 3 and are compared to other eucrites in Figures 7-8. Their major element abundances are similar to classical Main-Group eucrites, as shown by their FeO/MgO ratios and TiO_2 abundances, ranging respectively from 2.5 to 3 and 0.5 to 0.7 wt%. Their trace element abundances can be less typical, and are described for each textural group below.

3.2.1. Granulitic eucrites

The compositions of the four granulitic eucrites from Asuka (A-880702, A-880761, A-881388 and A-881467) are similar to the common Main-Group eucrites. They display flat REE patterns at about 10x CI, with (La/Sm)n ratios ranging from 0.92 to 1, and no noticeable Eu anomalies (Fig. 7). Clearly, they have not been significantly affected by Antarctic weathering (e.g., Mittlefehldt and Lindstrom, 2003).

Agoult is a very fresh Saharan find, with no chemical evidence of weathering (i.e., high Ba and Sr abundances, positive Ce anomalies, perturbed Th/U ratios (e.g., Barrat et al., 2003)). A small chip (sample A, 0.117 g) of Agoult was previously analyzed by Barrat et al. (2003). We have analyzed a second fragment (sample B, 0.6 g) from a different stone, that displays a more ferroan composition (Table 3). Both samples display flat REE patterns with small positive Eu anomalies (Eu/Eu* = 1.06-1.18). However, sample B exhibits a more pronounced positive Eu, and a noticeable light REE depletion ((La/Sm)n = 0.9). These features

are not the only differences between Agoult and typical Main-Group eucrites. In Figure 8, we have normalized the two Agoult samples to analyses of a large ophitic clast prepared from Juvinas (Barrat et al., 2007). Their trace element patterns display positive Sr anomalies. Furthermore, sample B displays low Th and light REE abundances, but normal Ba, Be, Ta abundances, and its Juvinas-normalized pattern shows a noticeable heavy REE enrichment.

3.2.2. A-87272

The two samples prepared from A-87272 display very similar major element abundances (Table 3). The situation is very different for the trace elements (Fig. 7). The first sample (,140) is characterized by low REE abundances more akin to cumulate eucrites rather than basaltic ones, a light REE-depleted pattern ((La/Yb)n=0.78), and positive Ce and Eu anomalies (Ce/Ce* = 1.09, Eu/Eu* = 1.62). The second one (,25) displays higher REE abundances, and a less perturbed REE pattern, with a smaller positive Eu anomaly (Eu/Eu* = 1.14). These features are clearly the fingerprint of Antarctic weathering (e.g., Floss and Crozaz, 1991; Mittlefehldt and Lindstrom, 1991, 2003), in agreement with Floss et al. (2000), who show that the A-87272 pyroxenes exhibit significant positive Ce anomalies. REE abundances in the A-87272 samples are not pristine and cannot be used to discuss its petrology.

3.2.3. DaG 945

DaG 945 shows the most unusual trace element abundances obtained during the course of this study. As shown by its Juvinas-normalized trace element pattern (Fig. 8), its Ba, Th, Ta (Nb), Sr, Hf (Zr), Eu, Ti and Li abundances resemble those of typical Main-Group eucrites, but its light REE abundances are low. Furthermore, this meteorite displays an unusual REE pattern (Fig. 7), with low light REE abundances at about 4x CI, a large positive Eu anomaly (Eu/Eu* = 1.95), and a strong heavy REE enrichment ((Gd/Yb)n = 0.61).

3.2.4. NWA 2362

Like DaG 945 and Agoult, NWA 2362 is a fresh Saharan find that displays no significant evidence of terrestrial weathering (i.e., Ba or Sr enrichments). However, its incompatible trace element abundances are unusual. Firstly, this eucrite is depleted in light REEs ((La/Sm)n = 0.77). Its REE pattern (Fig. 7) exhibits a pronounced positive Eu anomaly (Eu/Eu* = 1.31), which bears some resemblance to cumulate eucrites such as Moore County (e.g., Barrat et al., 2000). In a similar way to DaG 945, NWA 2362 displays an irregular Juvinas-normalized trace element pattern (Fig. 8), with positive Be, Sr, Hf, Eu, Ti anomalies and a pronounced heavy REE enrichment (Fig. 8).

3.3 Oxygen isotopes

Results of oxygen isotopic analysis (Table 4) show that all eight metamorphosed eucrites plot within 3σ of the Eucrite Fractionation Line (EFL) ($\Delta^{17}O = -0.239 \pm 0.007‰$ (1 σ)) (Fig.9) defined by Greenwood et al. (2005), indicating that they are isotopically normal HED meteorites. Despite the trace element evidence that A-87272 has experienced some Antarctic weathering (section 3.2.2), its oxygen isotope analysis plots close to the EFL at the isotopically heavy end of the basaltic eucrite array (Fig. 9), suggesting that A-87272 has experienced minimal terrestrial oxygen contamination. Compared to the other samples studied A-881467 and A-880761 have somewhat less negative $\Delta^{17}O$ values, which may reflect the influence of Antarctic weathering. To examine this possibility these two samples were leached in a solution of ethanolamine thioglycolate (EATG) (Cornish and Doyle, 1984), which removes iron oxides, hydroxides and metallic iron, but not silicate-bound iron. The oxygen isotope composition of the two EATG leached samples plot closer to the EFL (Table 4, Fig. 9) indicating that the untreated samples do contain terrestrial weathering products. If the EATG

treated samples are taken as being representative of the pre-weathered composition of A-881467 and A-880761, then all the samples analyzed in this study plot within 2σ of the EFL. The granulitic eucrites A-881388, A-880702, Agoult, A-881467 (EATG) and A-880761 (EATG), plus NWA 2362 are somewhat isotopically light with respect to $\delta^{18}O$ compared to the majority of the basaltic eucrites analyzed by Greenwood et al. (2005) (Fig. 9). This feature may indicate preferential removal of a high $\delta^{18}O$ component, which would leave the residual material isotopically light compared to normal eucrites. Silica minerals in eucrites are known to have $\delta^{18}O$ values of up to 14.2‰ (Taylor et al., 1965), while plagioclase has somewhat higher $\delta^{18}O$ values than pyroxene (Clayton, 1993). According to the phase diagram of Stolper (1977) early partial melts of eucrites would be rich in silica. Removal of such a melt would result in a decrease in the $\delta^{18}O$ value of the residual material. Although this effect is subtle, and for the Antarctic samples could be explained by small degrees of terrestrial weathering, the fact that two of the three hot desert finds also plot in the same low $\delta^{18}O$ region suggests that weathering may not be a significant factor. Thus, the oxygen isotope data appears to support the possibility that a melt component may have been extracted from at least some of the metamorphosed eucrites. In contrast, DaG 945 plots centrally within the basaltic eucrite array and A-87272 at the high $\delta^{18}O$ end. While it is possible that these samples have also lost a high $\delta^{18}O$ component i.e. their pre-metamorphic composition was isotopically heavier than their measured values, the oxygen isotope data does not provide any evidence with which to evaluate such a scenario.

4. Discussion

4.1. Thermal history of eucrites

In this section we use mineralogical evidence to constrain the thermal history of eucrites in order to understand crustal formation processes on Vesta. The vestiges of basaltic

texture and/or remnant Ca-zoning in pyroxenes seen in a number of samples indicate that the eucrites examined here crystallized rapidly in lava flows, or shallow intrusions. In this they resemble most basaltic eucrites (e.g., Takeda and Graham, 1991; Yamaguchi et al., 1996). Yamaguchi et al. (1996; 1997b) suggested that they were metamorphosed to varying degrees by burial during the formation of the primary crust. These eucrites experienced impact events, which caused brecciation, melting, and short-reheating, as well as cooling by excavation. These impact events occurred before, during, after thermal metamorphism (Metzler et al., 1995; Yamaguchi et al., 1996).

Pyroxenes in all the samples studied show exsolution textures and have homogeneous Fe/Mg ratios in low-Ca pyroxenes, indicating metamorphic equilibration at ~700-1000 °C, as is typically observed in basaltic eucrites (Takeda and Graham, 1991; Miyamoto et al., 1985; Yamaguchi et al., 1996). The presence of remnant Ca zoning in pyroxene suggests that the type A granulites, as well as eucrites A-87272, and DaG 945, were metamorphosed at lower temperatures (~800-900 ºC) than was the type 5 eucrite NWA 2362 (~1000 ºC) (Yamaguchi et al., 1996). However, the type A granulites are finer-grained (~0.1 mm) whereas A-87272, and DaG 945 are coarse-grained (~1-2 mm). Thus, the chemical equilibration of coarse pyroxene crystals in A-87272 and DaG 945 would have required a much longer time at the same given temperature (Miyamoto et al., 1985). The Wo content of low-Ca pyroxenes in A-87272 and NWA 2362 is extremely low ($Wo_{2.2}$ and $Wo_{2.7}$ for A-87272 and NWA 2362, respectively) compared to the other eucrites ($Wo_{\sim 4\text{-}5}$) (Fig. 4). The low Wo content is consistent with the fact that pigeonite in A-87272 is partially inverted to orthopyroxene. Thus, A-87272 and NWA 2362 experienced a longer duration of annealing and cooled extremely slowly to lower temperatures (Ishii and Takeda, 1974; Takeda and Graham, 1991), consistent with the presence of quartz, a low temperature form of silica, in these eucrites. On the other hand, the eucrites (e.g., type A granulites) with a relatively high Wo content ($Wo_{\sim 4\text{-}5}$) in pyroxene cooled more rapidly, probably because of impact exhumation.

NWA 2362 does not have remnant Ca zoning in pyroxene (i.e., type 5). This rock was metamorphosed at ~1000 ºC for an extended period (~0.1-1 Myr) to homogenize Ca-Mg in pyroxenes (Miyamoto et al., 1985).

Plagioclase in the type B granulitic eucrites and A-87272 show limited compositional variation, whereas type A granulitic eucrites, as well as DaG 945 and NWA 2362 show more extensive variation and a correlation between Na and K , indicating at least partial preservation of original igneous zoning (Fig. 5). The remnant basaltic textures, remnant Ca-zoning in pyroxene, and bulk Na and Ca abundances similar to that in normal basaltic eucrites all suggest that plagioclase in type B granulitic eucrites and A-87272 must originally have had igneous zoning. However, the limited plagioclase compositions are difficult to explain simply by metamorphic equilibration. Homogenization of Na-Ca zoning in plagioclase is an exceptionally slow processes because it requires reconstruction of SiO_4 tetrahedron (e.g., Morse, 1984). The Na-Ca diffusion coefficients in plagioclase are 4 orders of magnitude smaller than those of Ca in pigeonite (Grove et al., 1994; Miyamoto et al., 1985; Miyamoto and Takeda, 1994). Thus, if plagioclase was equilibrated by metamorphism, we would not expect remnant Ca zoning in pyroxene, whereas, for example, pyroxenes in A-87272 display remnant Ca zoning. Therefore, it is unlikely that plagioclase compositions were homogenized by metamorphic equilibration alone. In addition to metamorphic processes, we envisage that Na- (and K-) rich rims to zoned plagioclase were partially melted and removed. Reaction between the solid plagioclase core and partial melt resulted in reduced chemical variation in the residual feldspar. Both shock and metamorphic heating may have been involved in this partial melting process. The high K_2O abundances in tridymite (~0.1-0.2 wt%, Table 2) may also be due to this process, with the K_2O being derived from partial melts formed by fusion of plagioclase rims. Thus, the limited plagioclase compositions could be the result of short but high temperature heating events, accompanied by partial melting.

Spinel compositions in the eucrites studied here vary from low to high Ti, except

for those of NWA 2362 (Fig. 6). Enrichment of Ti in spinel is a typical feature of highly metamorphosed eucrites e.g. EET 90020 and Y-86763 (Floss et al., 2000; Yamaguchi et al., 2001). The close association of spinel and ilmenite is an indicative decomposition product of ulvöspinel (e.g., El Goresy and Ramdohr, 1975). Ti-rich spinel is unlikely to be an early primary phase formed during initial crystallization of eucrites. Instead the primary spinel in eucrites is typically chromite (Stolper et al., 1977), which is rich in Al and Cr with relatively high Fe/Mg (Yamaguchi, 2000). Ti-rich spinel is likely to be a metamorphic product. Experiments suggest that eucritic partial melts are enriched in Ti and Fe due to preferential melting of phases from the mesostasis (e.g., silica minerals, ilmenite, and Ca-phosphates) (Yamaguchi and Mikouchi, 2005). It is likely that partial melts enriched in Fe and Ti will crystallize ulvöspinel, which may subsequently decompose to chromite and ilmenite with minor Fe (Yamaguchi et al., 2001). Therefore, we suggest that the original Ti-rich spinel observed in highly metamorphosed eucrites crystallized from partial melts formed by reheating. In addition, the variation of Ti in spinels in individual eucrites implies disequilibrium processes (rapid cooling). The low Ti abundance in NWA 2362 spinel (Fig. 6) is problematic if this eucrite experienced a partial melting event. NWA 2362 has a large depletion of light REE possibly due to removal of a significant amount of partial melt (see below). Alternatively, crystallization of partial melts in NWA 2362 took place under different redox conditions, crystallizing chromite and ilmenite instead of ulvöspinel (e.g., El Goresy and Ramdohr, 1975).

In unmetamorphosed eucrites (type 1-2), silica-rich mesostasis occurs as glassy material interstitial to pyroxene and plagioclase (Takeda and Graham, 1991). In highly metamorphosed eucrites, silica minerals occur as fine-grained relict mesostasis or as isolated grains. In some eucrites (e.g., A-881467, A-881388 and EET 90020), silica minerals form large irregular grains and/or tridymite laths (Yamaguchi et al., 2001; this work). These mesostasis features may result from post crystallization reheating. Mesostasis is an

assemblage of the last crystallizing phases, thus it is most easily affected by post-crystallization reheating. The lath-shaped tridymite grains could crystallize directly from melt, or have coarsened in the presence of small amounts of melt. The enrichment of tridymite grains in minor elements (e.g., K, Al and Fe) was probably the result of metamorphic heating/melting of zoned pyroxene and plagioclase (see above). Small amounts of partial melt would have crystallized ulvöspinel and Ca-phosphate (Yamaguchi and Mikouchi, 2005). However, these phases are not always associated with each other. If the degree of melting is very small, and melt is distributed along grain boundaries and fractures, the distribution of these phases will depend on the nucleation sites in the rocks. A-87272 and NWA 2362 contain quartz which may have been produced during a phase transition and reflects a long period of low temperature metamorphism (<863 °C).

We suggest that the thermal histories of metamorphosed eucrites can be explained by a combination of prolonged thermal metamorphism interspersed with short duration reheating and cooling events. Homogenization, inversion and exsolution of pyroxene require extended time periods (e.g., 0.1-1 Ma) at 800-1000 °C (Miyamoto et al., 1985; Yamaguchi et al., 1996). In addition, the transition from tridymite to quartz takes place over a long period of time at low temperature. In contrast, the crystallization of large tridymite grains and Ti-rich spinels can be explained by a small degree of partial melting and subsequent recrystallization caused by short reheating events at >~1100 °C (Yamaguchi et al., 2001). Therefore, we suggest that short reheating events would have been superimposed on the crust-wide metamorphism that caused the pyroxene equilibration (see below).

4.2. Chemical compositions

From a chemical standpoint, two types of eucrite have been analyzed during the course of this study. Firstly, the granulitic eucrites from Asuka (A-880702, A-880761, A-881388, A-881467), which exhibit flat REE patterns, and are similar to common

Main-Group eucrites (the A-87272 eucrite whose trace element distribution clearly shows the effects of Antarctic weathering, also belongs to this group). Secondly, the Saharan eucrites Agoult, DaG 945 and NWA 2362, which display unusual incompatible trace element distributions, and in particular light REE depletions and positive Eu anomalies. These features are not restricted to these rare Saharan finds. Mittlefehldt and Lindstrom (2003) have analyzed EET 90020, another eucrite from Antarctica that displays a light REE depletion and a positive Eu anomaly as pronounced as DaG 945 (Fig. 7).

Four processes can be invoked to explain the development of a light REE depletion and a positive Eu anomaly in noncumulate eucrites: (i) weathering effects, (ii) plagioclase accumulation or oversampling of plagioclase, (iii) undersampling of phosphate in the analyzed samples, and finally (iv) partial melting and subsequent melt extraction.

Weathering effects

Terrestrial weathering can substantially modify the composition of meteorites. Since the 1980s, it has been amply demonstrated that cold desert weathering can generate abnormal trace element distributions in meteorites (Shimizu et al., 1984; Floss and Crozaz, 1991; Mittlefehldt and Lindstrom, 1991, 2003; Crozaz et al., 2003). Many eucrites recovered from the Antarctica blue ice fields display abnormal REE abundances decoupled from less mobile IEs (such as Ta, Zr, Eu, or Hf). Furthermore, their REE patterns frequently display positive or negative Ce anomalies, or unexpected positive Eu anomalies. These features have been ascribed to the dissolution of REE-rich phosphates by water equilibrated with the atmosphere (Mittlefehldt and Lindstrom, 1991). Ce can be oxidized to the +4 state, and in this way becomes fractionated from the +3 charged REEs. A-87272 is a perfect illustration of the effects of Antarctic weathering (see above). The weathering of achondrites in hot deserts can in principle generate similar effects, but the situation in such an environment is more complex. A variety of secondary minerals such as calcite, gypsum and Fe-hydroxides fill the

fractures of the meteorites, and can have a severe impact on the budget of some elements. As a consequence, hot desert finds often display a striking Ba and Sr enrichment. Light REE can be added to the system as well, but such an enrichment is easily found in light REE-poor meteorites (e.g., Barrat et al., 1998; 2006, 2008), and less frequently detected in richer systems such as eucrites. To date, only one sample (NWA 047) displays spurious light REE enrichments (Barrat et al., 2003). The three Saharan eucrites analyzed here (Agoult, DaG 945 and NWA 2362) are relatively fresh to very fresh finds, and the fingerprints of hot desert effects on the REE abundances are certainly insignificant. In conclusion, it would appear that hot-desert alteration cannot account for the light REE depletions and positive Eu anomalies shown by these eucrites.

Accumulation or oversampling of plagioclase

Plagioclase crystals found in eucrites display large positive Eu anomalies ((Eu/Sm)n >30 typically, Hsu and Crozaz, 1996; Floss et al., 2000). A small accumulation of plagioclase in a eucritic melt can potentially be the cause of a positive Eu anomaly measured in a bulk sample. Similarly, a positive Eu anomaly can be measured if the analyzed sample is not representative and contains too much plagioclase (case of very small chips). However, these possibilities cannot account for the large Eu anomalies displayed for example by NWA 2362 and DaG 945:

- Our powders have been prepared from large chips (>0.6 g), and oversampling of plagioclase is unlikely.
- Plagioclase in eucrites is light REE enriched and, except for Eu, displays low REE abundances (Hsu and Crozaz, 1996; Floss et al., 2000). As a consequence, the addition of plagioclase to a eucritic melt (or oversampling of this phase) would not generate an overall light REE depletion.
- We have estimated the amount of plagioclase necessary to explain positive anomalies

using typical eucrite (Sm = 1.7 µg, Eu = 0.63 µg) and plagioclase (Sm = 0.1 µg, Eu = 1.0 µg Floss et al., 2000) abundances. About 20 % and 40 % of accumulated plagioclase are necessary to explain Eu anomalies as pronounced as those measured in NWA 2362 and DaG 945 respectively. If real, such proportions of plagioclase would significantly affect the Al concentrations of the bulk rocks, and high Al_2O_3 abundances should be observed (Al_2O_3 > 15 wt%). Instead, the Al_2O_3 abundances in DaG 945, NWA 2362 and in all the other samples in this study (Al_2O_3= 11.7 – 13.7 wt%) are similar to the concentrations of Main-Group eucrites such as Juvinas (Al_2O_3= 12.9 wt%, Barrat et al., 2007).

In conclusion, the positive Eu anomalies shown by these highly metamorphosed eucrites cannot be explained either by plagioclase accumulation or plagioclase oversampling.

Undersampling of Ca-phosphates

Fluorapatite and merrilite are major carriers of REEs in eucrites. Hsu and Crozaz (1996) have estimated that these phosphates account for more than 90 % of the whole-rock light REE abundances, more than 25 % of the Eu, and more than 80 % of the heavy REE abundances, despite their low modal abundance (<0.1-0.4 vol%, e.g., Delaney et al., 1984). As pointed out by Hsu and Crozaz (1996), the heterogeneous distribution of phosphate can have a significant impact on whole rock analyses, especially when small amounts of sample are used. An excess of phosphate in a sample can account for high REE abundances, a light REE enrichment and a pronounced negative Eu anomaly (Fig. 10). Conversely, a deficit of phosphate can account for low light REE abundances, a light REE depletion and a large positive Eu anomaly. The amount of phosphate required to produce these effects is small, and is hardly detectable using the P abundances alone. In Figure 10, the patterns of the light REE depleted eucrites are well reproduced by a limited undersampling of phosphates, and one might conclude that their characteristic patterns result from inhomogeneous distribution of accessory phases in the samples. However, we do not favor this interpretation for the

following reasons:

- Agoult is a fine-grained unbrecciated eucrite that contains numerous small phosphate grains (<10-20 μm). Chemical mapping indicates that these crystals are fairly evenly distributed, and consequently our powder, prepared with a 0.6 g-sample, is certainly representative of the meteorite as whole.
- DaG 945 and NWA 2362 are both coarser grained and have more pronounced light REE depletions and positive Eu anomalies than Agoult. For both rocks, the powders were prepared using larger chips (1.7 g for DaG, 2 g for NWA 2362), significantly larger than the chips usually used in geochemical studies of eucrites, and again certainly representative of the whole meteorite.

It is important to note that among the numerous fractions of unweathered eucrites so far analyzed, most of them prepared from small chips, light REE depleted samples are exceptional, and REE abundances are, for the vast majority of the cases, consistent with major or other trace element concentrations. This evidence suggests that, usually, phosphates are correctly sampled in 0.1-0.2 g splits, probably because these phases occur mostly as small to very small crystals. Hence, the light REE depletions displayed by some eucrites are more likely related to a petrogenetic process rather than an artifact produced by an undersampling of phosphate phases.

Partial melting and extraction of the melts

When a eucrite is heated to a temperature slightly above its solidus for a short period (i.e., about 1050 °C for 24 hours), a small fraction of melt (< 1 %) is produced that can move along preexisting fractures (Yamaguchi and Mikouchi, 2005). Such a process could have been operative during the genesis of some highly metamorphosed eucrites. It has been previously suggested that at least two of them, Y-86763 and EET 90020, have experienced partial melting (Floss et al., 2000; Yamaguchi et al., 2001).

Partial melting can have major effects on the trace element budget if a small fraction of melt is expelled from the rock. However, the chemical composition of a residual lithology is extremely difficult to model, and residues after partial melting of a eucrite are no exception. The preliminary data obtained by Yamaguchi and Mikouchi (2005) suggest that the composition of the first melt produced is strongly controlled by accessory phases, such as phosphates and ilmenite. Because phosphates are the main carriers of light REEs in eucrites (Delaney et al., 1984; Hsu and Crozaz, 1996), a severe depletion of these elements is expected in the residual lithology. Unfortunately, the available experimental data are insufficient to calculate rigorously its composition. We have calculated the REE abundance of the residues produced by the partial melting of a eucrite (60 % pyroxene, 40 % plagioclase). We have used the Main-Group eucrite Juvinas as a starting composition, and the same parameters as Barrat et al. (2007) for the melting model (see pages 4118-4119, Barrat et al., 2007). As emphasized previously (Barrat et al., 2007), these calculations are somewhat simplified because the involvement of phosphate and of other accessory phases, which would be important at very low degrees of melting, are not taken into account here. However, these calculations certainly provide a realistic picture of the important features of the residues. The REE patterns of the residues obtained after 1 to 10 % partial melting are shown in Figure 11. They display a light REE depletion and a marked positive Eu anomaly. Importantly, the calculated patterns are a close match to those displayed by some highly metamorphosed eucrites, including EET 90020.

Therefore, we conclude that partial melt formation and removal is the mostly likely mechanism to explain the light REE depletions seen in A-87272, Agoult, DaG 945, and NWA 2362. Results from oxygen isotope analysis (section 3.3) also support the view that a melt component has been extracted from at least some of these metamorphosed eucrites. We propose that these partially melted eucrites, "residual eucrites", are the third chemical group of basaltic eucrites; the others being Main-Group - Nuevo Laredo trend and Stannern trend

eucrites. The chemical relationships among these three groups are nicely shown in the La-Sc diagram (Fig. 12). Stannern trend eucrites plot at the opposite end of the diagram to the residual eucrites, with Main-Group eucrites in the middle. We suggest that these groups are genetically related as discussed below.

4.3. Implications for the Geologic history of Vestian crust

Barrat et al. (2007) suggested that contamination of Main-Group eucrite magmas by melts derived by partial melting of the crust can explain the high incompatible trace element concentrations of Stannern trend eucrites. This model is consistent with the presence of the light-REE depleted eucrites (residual eucrites), which were probably deeply seated in the crust. This model predicts that Stannern and Main-Group – Nuevo Laredo trend eucrites would have been contemporaneously erupted. This is required because Stannern trend eucrites in our model represent crustally contaminated Main-Group-Nuevo eucrites. However, it is likely that Stannern trend eucrites formed relatively late in the magmatic history of Vesta. It is also a required feature of our model that metamorphism and crustal partial melting occurred simultaneous during the formation of Stannern trend eucrites.

What were the heat sources for the reheating events? Yamaguchi et al. (1996; 1997b) suggested that the eucrites were buried by repeated eruption and rapid accumulation of basalts, with metamorphism of significant volumes of eucrites taking place as a consequence of internal heating. However, the thermal histories of eucrites seem to be more complicated than would be expected from a simple burial model (Yamaguchi et al., 2001; Schwartz and McCallum, 2005; this work). Takeda and Graham (1991) suggest that metamorphism was caused by overlying lava flows and/or from impact events. Both processes do not work effectively near the surface at lower ambient temperatures (Keil et al., 1997; Yamaguchi et al., 1996). Intrusions of large hot plutons could be a possible mechanism. Such local processes would not be capable of heating up the entire crust to the range of

metamorphic temperatures seen in eucrites (~700-1000 °C) unless the heat is continuously supplied (Yamaguchi et al., 1996; Yamaguchi et al., 2001). However, at the high ambient temperatures likely to have been achieved in the early crust during burial metamorphism, these local processes might have provided favorable conditions for local partial melting.

We suggest that the thermal structure of the early eucritic crust was produced by burial metamorphism (global crustal metamorphism) with superimposed local reheating events (Fig. 13). Figure 13(A) describes thermal histories of eucrites by the simple burial metamorphism (Yamaguchi et al., 1996; 1997b). The degrees of reheating are related to the degree of burial (1a,b). At the bottom of the crust, close to the contact with the residual magma ocean partial melting zones may have developed (1a) (in the ocean itself temperatures would have exceeded the solidus at ~1100 °C) (Barrat et al., 2007). In contrast, most basaltic eucrites experienced sub-solidus annealing (1b). Figures 13B and 13C describe the effects of local heating events during the burial metamorphism (e.g., 1a). The local reheating events include magma intrusion (Fig. 13B) and impact events (Fig. 13C). Simple thermal calculations indicate that emplacement of eucritic magma (~1200 °C) into hot crust (~800-1000 °C) could easily cause partial melting of the country rocks (2a) (Fig. 13B). Larger intrusions cause more prolonged reheating than small intrusions. Moderate impact events at high temperatures may cause partial melting (3a and 3a') (Fig. 13C) (Yamaguchi et al., 2001; 2002). Impact events have similar effects to those of magma intrusions but have the potential to increase temperatures more rapidly. In some cases, impact events may cool already hot rocks by excavation (3a' and 3b') (Fig. 13C). Local reheating by magma intrusion or impact events would also have occurred at lower temperatures, but these processes would not have resulted in partial melting (2b, 3b, 3b') (Fig. 13B and C).

5. Conclusions

In order to better understand the thermal history and formation processes of Vesta's

crust, we have performed a detailed mineralogical and geochemical study of eight basaltic eucrites. These basaltic eucrites, are type 4-7, granulitic rocks and were metamorphosed at ~700-1000 °C for a prolonged time that caused equilibration of pyroxenes. Some of the eucrites (granulitic eucrites) experienced brecciation and impact melting before or during thermal metamorphism. Other eucrites experienced high temperature metamorphism that altered mesostasis mineralogy. Although typical basaltic eucrites show flat REE patterns, Agoult, A-87272, DaG 945, and NWA 2362 show varying degrees of light REE depletions with positive Eu anomalies. These REE patterns are rather similar to those of cumulate eucrites. However, the major element abundances and mineral chemistry of pyroxene and plagioclase are consistent with the fact that these rocks are normal basaltic eucrites. We suggest that the light REE depletions were caused by fusion and the subsequent extraction of the partial melts that were formed by this process. This interpretation is consistent with mineralogical evidence for high temperature metamorphism. The degree of light REE depletion and the metamorphic grade estimated from pyroxene mineralogy are not always consistent. We explain the absence of a simple correlation by the combination of prolonged metamorphism and short but high temperature reheating events. Equilibration, inversion and exsolution of pyroxene took place over a protracted interval at moderate temperatures, whereas the partial melting and the extraction of melt were short duration events.

The mineralogical and geochemical evidence from the eucrites studied here suggests that the crust of Vesta experienced a complex thermal history shortly after, or during its formation. Yamaguchi et al. (1996) suggested that the entire eucritic crust experienced global crustal metamorphism. Occasional impact events and emplacement of hot magmas would have locally heated up the eucritic country rocks. Deeply buried basalts in contact with the residual magma ocean would have been strongly heated, with some eucrites in these zones being partially melted. If it occurred during volcanism, the partial melts would have contaminated the Main-Group magma to produce the Stannern-trend eucrites. Thus, the

residual eucrites discussed in this paper are complementary to the Stannern trend eucrites. The magma ocean model, plus secondary re-processing of the primary crust can therefore explain both the range of metamorphic types, as well as the chemical groups, displayed by the basaltic eucrites.

Acknowledgements

This research was partly supported by Grant-in-Aid for Scientific Research from Ministry of Education, Science, and Technology, Japan and was initiated while one of the authors (AY) stayed in and U.B.O. in Brest. The PSSRI oxygen isotope laboratory is funded through an STFC rolling grant. The manuscript was significantly improved as result of helpful discussions with Dr. H. Takeda. J. Spray, E.R.D. Scott, and C. Floss are thanked for their constructive reviews, and R. Korotev for his efficient editorial handling. Jenny Gibson is thanked for her help with oxygen isotope analysis.

References

Arai T., Takeda H., Lofgren G.E. and Miyamoto M. (1998) Metamorphic transformation of opaque minerals in some eucrites. *Antarct. Meteor. Res.* **11,** 71-91.

Barrat J.A. (2004) Determination of the parental magmas of HED cumulates: The effects of interstitial melts. *Meteoritics Planet. Sci*. **39**, 1767-1779.

Barrat J.A., Yamaguchi A., Greenwood R.C., Bohn M., Cotten J., Benoit M. and Franchi A. (2007) The Stannern trend eucrites: Contamination of Main-Group eucritic magmas by crustal partial melts. *Geochim. Cosmochim. Acta* **71,** 4108-4124.

Barrat J.A., Beck P., Bohn M., Cotten J., Gillet Ph., Greenwood R.C. and Franchi I.A. (2006) Petrology and geochemistry of the fine-grained, unbrecciated diogenite Northwest Africa 4251. *Meteor. Planet. Sci.* **41,** 1045-1057.

Barrat J.A., Jambon A., Bohn M., Blichert-Toft J., Sautter V., Göpel C., Gillet Ph., Boudouma O., and Keller F. (2003) Petrology and geochemistry of the unbrecciated achondrite North West Africa 1240 (NWA 1240): an HED parent body impact melt. *Geochim. Cosmochim. Acta* **67**, 3959-3970.

Barrat J.A., Blichert-Toft J., Gillet Ph., and Keller F. (2000) The differentiation of eucrites: the role of *in-situ* crystallization. *Meteor. Planet. Sci.* **35**, 1087-1100.

Barrat J.A., Gillet Ph., Lesourd M., Blichert-Toft J. and Poupeau G.R. (1998) The Tatahouine diogenite: mineralogical and chemical effects of 63 years of terrestrial residence. *Meteoritics Planet. Sci.* **34**, 91-97.

Bermingham K.R., Norman M.D., Christy A.G. and Arculus R.J. (2008) A new variety of eucrite? Clues to early differentiation of igneous asteroid. *Lunar Planet. Sci.* XXXIX, #1225 (abstr.).

Binzel R.P. and Xu S. (1993) Chips off asteroid 4 Vesta: Evidence for the parent body of basaltic achondrite meteorites. Science **260,** 186-191.

Bizzaro et al. (2005) Rapid timescales for accretion and melting of differentiated planetsimals

inferred from ^{26}Al-^{26}Mg chronometry. *Astrophys. J.* **632,** L41-L44.

Clayton R.N. (1993) Oxygen Isotopes in Meteorites. *Annu. Rev. Earth Planet. Sci*. **21**, 115-149

Cotten J., Ledez A., Bau M., Caroff M., Maury R. C., Dulski P., Fourcade S., Bohn M. and Brousse R. (1995) Origin of anomalous Rare-Earth Element and Yttrium Enrichments in Subaerially Exposed Basalts—evidence from French-Polynesia. *Chem. Geol.* **119**(1-4), 115–138.

Cornish L. and Doyle A.M. (1984) Use of ethanolamine thioglycollate in the conservation of pyritised fossils.*Palaeontology* 27, 421-424.

Crozaz G., Floss C. and Wadhwa M. (2003) Chemical alteration and REE mobilization in meteorites from hot and cold deserts. *Geochim. Cosmochim. Acta* **67,** 4727-4741.

Delaney J.S., Prinz M. and Takeda H. (1984) The polymict eucrites. *Proc. Lunar Planet. Sci. Conf.* **15,** *J. Geophys. Res.* **89,** C251–C288.

Ebihara M., Oura Y., Ishii T., Setoguchi M., Nakahara H. and Otsuki T. (2000) How effectively is the photon activation analysis applied to meteorite samples? *J. Radioanal. Nucl. Chem.* **244,** 491-496.

El Goresy A. and Ramdohr P. (1975) Subsolidus reduction of lunar opaque oxides: Textures, assemblages, geochemistry, and evidence for a late-stage endogenic gaseous mixture. *Proc. Lunar Sci. Conf.* **6,** 729–745

Evensen N.M., Hamilton P.J. and O'Nions R.K. (1978) Rare Earth abundances in chondritic meteorites. *Geochim. Cosmochim. Acta* **42,** 1199-1212.

Floss C., Crozaz G., Yamaguchi A. and Keil K. (2000) Trace element constraints on the origins of highly metamorphosed Antarctic eucrites. Antarct. Meteorite Res. 13, 222-237.

Floss C. and Crozaz G. (1991) Ce anomalies in the LEW85300 eucrite: evidence for REE mobilization during Antarctic weathering. *Earth Planet. Sci. Lett.* **107,** 13-24.

Greenwood R.C., Franchi I.A., Jambon A., Barrat J.A. and Burbine T.H. (2006) Oxygen

isotope variation in stony-iron meteorites. *Science* **313,** 1763-1765.

Greenwood R.C., Franchi I.A., Jambon A. and Buchanan P.C. (2005) Widespread magma oceans on asteroidal bodies in the early Solar System. *Nature* **435,** 916-918.

Grove T.L., Barker M.B. and Kinzler R.J. (1994) Grove T. L., Baker M. B., and Kinzler R. J. (1984) Coupled CaAl-NaSi diffusion in plagioclase feldspar: Experiments and application to cooling rate speedometry. *Geochim. Cosmochim. Acta* **48,** 2113–2121.

Harlow G.E and Klimentidies R. (1980) Clouding of pyroxene and plagioclase in eucrites: Implications for post-crystallization processing. *Proc. Lunar Planet. Sci. Conf.* **11th,** 1131-1143.

Hsu W. and Crozaz G. (1996) Petrogenesis of eucrites I: Non-cumulate eucrites. *Geochim. Cosmochim. Acta* **60**(22), 4571-4591.

Ishii T. and Takeda H. (1974) Inversion, decomposition and exsolution phenomena of terrestrial and extraterrestrial pigeonite. *Mem. Geol. Soc. Japan* **11,** 19-36.

Keil K., Stöffler D., Love S. G. and Scott E. R. D. (1997) Constraints on the role of impact heating and melting in asteroids. *Meteor. Planet. Sci.* **32,** 349–363.

Latif S. A., Oura Y., Ebihara M., Kallemeyn G. W., Nakahara H., Yonezawa C., Matsue T. and Sawahata H. (1999) Prompt gamma-ray analysis (PGA) of meteorite samples, with emphasis on the determination of Si. *J. Radioanal. Nucl. Chem.* **239,** 577-580.

Mayne R.G., McSween Jr H.Y., McCoy T.J., and Gale A. (2009) Petrology of the unbrecciated eucrites. *Geochim. Cosmochim. Acta* **73,** 794-819.

McCord T.B., Adams J.B. and Johnson T.V. (1970) Asteroid Vesta: Spectral reflectivity and compositional implications. *Science* **168,** 1445-1447.

Metzler K., Bobe K., Palme H., Spettel B., and Stöffler D. (1995) Thermal and impact metamorphism on the HED parent asteroid. *Planet. Space Sci.* **43**, 499-525.

Miller M. F., Franchi A., Sexton A. S. and Pillinger C. T. (1999) High precision $\delta^{17}O$ measurements of oxygen from silicates and other oxides: method and applications. *Rapid*

Commun. Mass Spectrom. **13,** 1211–1217.

Misawa K., Yamaguchi A. and Kaiden H. (2006) U–Pb and ^{207}Pb–^{206}Pb ages of zircons from basaltic eucrites: Implications for early basaltic volcanism on the eucrite parent body. *Geochim. Cosmochim. Acta* **69,** 5847–5861.

Mittlefehldt D.W. and Lindstrom M.M. (2003) Geochemistry of eucrites: genesis of basaltic eucrites, and Hf and Ta as petrogenetic indicators for altered Antarctic eucrites. *Geochim. Cosmochim. Acta* **67**, 1911-1935.

Mittlefehldt D.W., McCoy T.J., Goodrich C.A., and Kracher A. (1998) Non-chondritic meteorites from asteroidal bodies. in *"Planetary Materials" (J.J. Papike, editor)*, *Rev. Miner.* **36**, chapter 4, 1-195.

Mittlefehldt D.W. and Lindstrom M.M. (1991) Generation of abnormal trace element abundances in Antarctic eucrites by weathering processes. *Geochim. Cosmochim. Acta* **55,** 77-87.

Miyamoto M. and Takeda H. (1994) Evidence for excavation of deep crustal material of a Vesta-like body from Ca compositional gradients in pyroxene. *Earth Planet. Sci. Lett.* **122,** 343–349.

Miyamoto M., Duke M. B. and Mckay D. S. (1985) Chemical zoning and homogenization of Pasamonte-type pyroxene and their bearing on thermal metamorphism of Howardite parent body. *Proc. Lunar Planet. Sci. Conf.* **15,** C629-C635.

Mori H. and Takeda H. (1985) Oriented chromite inclusions in pigeonite crystals of eucrite meteorites. *Papers presented on NIPR Symp. Antarct. Meteorites* **10,** 26-28 (abstr.).

Morse S. A. (1984) Cation diffusion in plagioclase feldspar. *Science* **225,** 504–505.

Nyquist L. E., Takeda H., Bansal B. M., Shih C.-Y., Wiesmann H., and Wooden J. L. (1986) Rb-Sr and Sm-Nd internal isochron ages of a subophitic basalt clast and a matrix sample from the Y75011 eucrite. *J. Geophys. Res.* **91,** 8137–8150.

Righter K. and Drake M.J. (1997) A magma ocean on Vesta: core formation and petrogenesis

of eucrites and diogenites. *Meteoritics Planet. Sci* **32**, 929-944.

Righter K. and Drake M.J. (1996) Core formation in Earth's moon, Mars, and Vesta. *Icarus* **124,** 513-529.

Schwartz J.M. and McCallum I.S. (2005) Comparative study of equilibrated and unequilibrated eucrites: Subsolidus thermal histories of Haraiya and Pasamonte. *American Mineralogist* **90,** 1871-1886.

Scott E.R.D., Taylor G.J., Newsom H.E., Herbert F., Zolensky M.E. and Kerridge J.F. (1989) Chemical, thermal, and impact processing of asteroids, in Asteroid II (edited by R.P,. Binzel, T. Gehrels and M.S. Matthews), pp. 701-739. University of Arizona Press, Tucson

Shimizu H., Tanaka T. and Masuda A. (1984) Meteoritic $^{138}Ce/^{142}Ce$ ratio and its evolution. *Nature* **307,** 251–252.

Shinotsuka K., Hidaka H., Ebihara M. and Nakahara H. (1996) ICP-MS analysis of geological standard rocks for Yttrium, Lanthanoids, Thorium and Uranium. *Anal. Sci.* **12,** 917-922.

Shirai N. and Ebihara M. (2004) Chemical characteristics of a Martian meteorite, Yamato 980459. *Antarct. Meteorite Res.* **17,** 55-67.

Stolper E. (1977) Experimental petrology of eucrite meteorites. *Geochim. Cosmochim. Acta* **41**, 587-611.

Takeda H. (1997) Mineralogical records of early planetary processes on the howardite, eucrite, diogenite parent body with reference to Vesta. *Meteoritics and Planet. Sci.* **32,** 841-853.

Takeda H., Ishii T., Arai T. and Miyamoto M. (1997) Mineralogy of the Asuka 87 and 88 eucrite and crustal evolution of the HED parent body. *Antarct. Meteorite Res.* **10,** 401-413.

Takeda H. and Graham A.L. (1991) Degree of equilibration of eucritic pyroxenes and thermal metamorphism of the earliest planetary crust. *Meteoritics* **26**, 129-134.

Taylor H. P. Jr., Duke M.B., Silver L.T and Epstein S. (1965) Oxygen isotope studies of minerals in stony meteorites. *Geochim. Cosmochim. Acta* **29**, 489-512.

Treiman A.H. (1997) The parent magmas of the cumulate eucrites: A mass balance approach. Meteor. Planet. Sci. 32, 217-230.

Warren P.H, and Jerde E. (1987) Composition and origin of Nuevo Laredo trend eucrites. *Geochim. Cosmochim. Acta* **51**, 713-725.

Warren P. H. and Kallemeyn G. W. (2001) A correlation between erupted lava composition and degree of subsequent thermal metamorphism for HED-meteoritic basalts. *Antarctic Meteorites* **XXVI**, 154-155 (abstr.).

Yamaguchi A. (2000) Spinels in basaltic eucrites: implication for crystallization and metamorphic history. *Meteoritics Planet. Sci.* **35**, A174 (abstr.).

Yamaguchi A., Barrat J.A., Shirai N., Okamoto C., Setoyanagi T. and Ebihara M. (2007) Highly metamorphosed eucrites, A-87272 and DaG 945: Residues after crustal partial melting. *Meteoritics Planet. Sci.* **42,** A167 (abstr.)

Yamaguchi A. and Mikouchi T. (2005) Heating experiments of the HaH 262 eucrite and implication for the metamorphic history of highly metamorphosed eucrites. *Lunar and Planetary Science* **36**, CD#1574 (abstr.).

Yamaguchi A., Sekine T. and Mori H. (2002) Shock experiments on a preheated basalt. In High-Pressure Shock Compression of Soid V, Shock Chemistry with Applications to Meteorite Impact pp. 29-45 (Chapter 2). Springer.

Yamaguchi A., Taylor G. J., Keil K., Floss C., Crozaz G., Nyquist L.E., Bogard D.D., Garrison D., Reese Y., Wiesmann H. and Shih C.Y. (2001) Post-crystallization reheating and partial melting of eucrite EET90020 by impact into the hot crust of asteroid 4Vesta ~4.50 Ga ago. *Geochim. Cosmochim. Acta* **65**, 3577-3599.

Yamaguchi A., Taylor G.J. and Keil K. (1997a) Shock and thermal history of equilibrated eucrites from Antarctica. *Antarct. Meteorite Res.* **10,** 415-436.

Yamaguchi A., Taylor G.J. and Keil K. (1997b) Metamorphic history of the eucritic crust of 4 Vesta. *J. Geophys. Res.* **102,** 13381-13386.

Yamaguchi A., Taylor G.J., and Keil K. (1996) Global crustal metamorphism of the eucrite parent body. *Icarus* **124**, 97-112.

Yamaguchi A., Takeda H., Bogard D.D. and Garrison D. (1994) Textural variations and impact history of the Millbillillie eucrite. *Meteoritics* **29,** 237-245.

Yanai K. and Kojima H. (1995) *Catalog of the Antarctic meteorites,* 230 pp. National Institute of Polar Research, Tokyo.

Table 1. Petrologic and chemical properties of eucrites studied here and EET 90020 and Juvinas for comparison.

Name	Type	Petrographic texture	Pyroxene textures	La/Yb (CI)	Reference
A-880702	Gra (type A)	Granulitic	Remnant Ca-zoning	1.11	[1]
A-881467	Gra (type A)	Granulitic	Remnant Ca-zoning	0.90	[1]
A-880761	Gra (type A)	Granulitic	Homgeneous low-Ca pyx & aug	1.13	[1]
A-881388	Gra (type B)	Granulitic	Homgeneous low-Ca pyx & aug	1.07	[1]
Agoult	Gra (type B)	Granulitic	Homgeneous low-Ca pyx & aug	0.78-0.92	[1]
A-87272	Type 7	Gabbroic	Remnant Ca-zoning, partly inverted to opx	0.78-0.99	[1]
DaG 945	Type 4	Subophitic	Remnant Ca-zoning	0.51	[1]
NWA 2362	Type 5	Subophitic to gabbroic	Homogeneous low-Ca pyx	0.69	[1]
EET 90020	Type 5	Subophitic	Homogeneous low-Ca pyx	0.31-0.35	[2]
Juvinas	Type 5	Subophitic to gabbroic	Homogeneous low-Ca pyx	1.03	[3]

[1] This work; [2] Mittlefehldt and Lindstrom (2003); [3] Barrat et al. (2000)

Table 2. Chemical compositions (wt%) of phases.

		SiO_2	TiO_2	Al_2O_3	Cr_2O_3	FeO	MnO	MgO	CaO	Na_2O	K_2O	Total		
Pyroxenes													Wo	En
A-880702 (Gra-A)	*Low-Ca*	50.2	0.20	0.23	0.11	37.2	1.14	11.2	1.15	0.03	0.00	101.4	2.53	33.96
	High-Ca	51.4	0.34	0.60	0.25	18.3	0.49	9.39	19.7	0.04	0.01	100.6	41.91	27.76
A-881467 (Gra-A)	*Low-Ca*	50.4	0.24	0.24	0.13	35.6	1.15	11.4	1.95	0.07	0.01	101.2	4.27	34.84
	High-Ca	51.1	0.42	0.71	0.28	18.6	0.48	9.38	19.3	0.07	0.01	100.3	41.14	27.87
A-880761 (Gra-B)	*Low-Ca*	51.0	0.24	0.21	0.08	35.5	1.11	12.2	1.40	0.00	0.01	101.8	3.04	36.76
	High-Ca	51.5	0.37	0.65	0.29	17.5	0.54	10.2	19.3	0.07	0.01	100.5	41.00	30.02
A-881388 (Gra-B)	*Low-Ca*	50.8	0.21	0.23	0.07	34.3	1.09	12.6	1.40	0.00	0.00	100.6	3.08	38.31
	High-Ca	51.7	0.43	0.69	0.25	17.7	0.52	9.87	19.4	0.00	0.00	100.5	41.35	29.28
Agoult (Gra-B)	*Low-Ca*	50.2	0.22	0.22	0.10	35.1	1.13	12.1	1.70	0.01	0.00	100.7	3.70	36.66
	High-Ca	51.2	0.53	0.73	0.27	17.4	0.54	10.0	19.1	0.09	0.01	100.0	40.96	29.91
A-87272 (Type 7)	*Low-Ca*	50.1	0.10	0.19	0.08	36.1	1.15	12.3	0.90	0.04	0.03	101.0	1.94	37.15
	High-Ca	51.2	0.34	0.60	0.29	15.9	0.61	9.95	21.1	0.02	0.01	100.0	44.59	29.23
DaG 945 (Type 4)	*Low-Ca*	50.3	0.22	0.25	0.07	36.6	1.16	11.2	1.59	0.03	0.00	101.4	3.48	33.97
	High-Ca	51.0	0.47	0.73	0.33	18.7	0.51	9.28	19.3	0.05	0.00	100.4	41.17	27.60
NWA 2362 (Type 5)	*Low-Ca*	50.5	0.10	0.18	0.26	35.8	1.03	12.5	0.69	0.02	0.01	101.1	1.50	37.73
	High-Ca	51.8	0.37	0.81	0.39	14.8	0.48	10.5	21.7	0.03	0.00	100.8	45.43	30.47

(Continued)

		SiO_2	TiO_2	Al_2O_3	Cr_2O_3	FeO	MnO	MgO	CaO	Na_2O	K_2O	Total		
Plagioclase													*An*	*Or*
A-880702 (Gra-A)	High-An	46.4	0.00	34.6	0.00	0.07	0.00	0.02	18.3	1.17	0.07	100.6	*89.25*	*0.42*
	Low-An	47.4	0.02	33.7	0.00	0.13	0.00	0.02	17.2	1.70	0.16	100.4	*84.04*	*0.92*
A-881467 (Gra-A)	High-An	46.2	0.00	34.0	0.00	0.26	0.00	0.03	18.1	1.11	0.08	99.7	*89.52*	*0.48*
	Low-An	47.3	0.01	33.6	0.00	0.15	0.05	0.03	17.1	1.65	0.13	100.0	*84.50*	*0.79*
A-880761 (Gra-B)	av (n=24)	46.1	0.01	34.5	0.01	0.32	0.01	0.01	18.2	1.12	0.08	100.4	*89.57*	*0.48*
A-881388 (Gra-B)	av (n=27)	46.0	0.00	34.5	0.01	0.27	0.01	0.01	18.1	1.13	0.08	100.2	*89.43*	*0.50*
Agoult (Gra-B)	av (n=58)	46.2	0.01	34.4	0.01	0.28	0.02	0.02	18.0	1.16	0.06	100.2	*89.28*	*0.35*
A-87272 (Type 7)	av (n=38)	46.3	0.01	35.1	0.01	0.26	0.02	0.01	18.1	1.03	0.06	100.9	*90.36*	*0.35*
DaG 945 (Type 4)	Low-An	45.8	0.00	34.8	0.03	0.69	0.01	0.03	18.5	0.96	0.06	100.9	*91.09*	*0.35*
	High-An	48.0	0.01	33.1	0.00	0.32	0.00	0.00	16.6	1.75	0.15	99.9	*83.26*	*0.89*
NWA 2362 (Type 5)	Low-An	45.6	0.00	35.0	0.00	0.50	0.00	0.15	18.6	0.89	0.04	100.7	*91.81*	*0.22*
	High-An	47.1	0.02	34.4	0.02	0.95	0.00	0.75	17.3	1.33	0.08	102.0	*87.37*	*0.47*
Silica minerals														
A-880702 (Gra-A)	av (n=4)	99.0	0.07	0.27	0.00	0.24	0.03	0.01	0.03	0.01	0.18	99.9		
A-881467 (Gra-A)	av (n=4)	99.3	0.07	0.21	0.01	0.20	0.02	0.01	0.01	0.02	0.14	100.0		
A-880761 (Gra-B)	av (n=8)	98.7	0.09	0.23	0.01	0.24	0.01	0.00	0.03	0.02	0.15	99.4		
A-881388 (Gra-B)		98.2	0.09	0.23	0.01	0.15	0.00	0.00	0.02	0.03	0.14	98.9		
Agoult (Gra-B)	av (n=10)	98.9	0.10	0.27	0.00	0.19	0.01	0.00	0.04	0.03	0.14	99.7		
A-87272 (Type 7)	av (n=6)	98.7	0.05	0.19	0.01	0.21	0.02	0.01	0.03	0.02	0.08	99.3		
DaG 945 (Type 4)	av (n=5)	98.9	0.06	0.18	0.00	0.18	0.01	0.00	0.02	0.02	0.11	99.5		
NWA 2362 (Type 5)	av (n=11)	98.39	0.15	0.35	0.04	0.17	0.01	0.02	0.15	0.02	0.06	99.3		

(Continued)

		SiO2	TiO2	Al2O3	Cr2O3	FeO	MnO	MgO	CaO	V2O3	Total		
Spinel												Usp	Chr
A-880702 (Gra-A)	*LowTi*	0.00	6.27	7.65	46.9	37.0	0.61	0.70	0.04	0.90	100.1	17.0	66.8
	High Ti	0.03	17.8	3.33	28.0	48.6	0.73	0.56	0.06	0.62	99.8	50.7	41.9
A-881467 (Gra-A)	*LowTi*	0.01	10.6	5.75	40.0	41.2	0.61	0.75	0.03	0.71	99.6	29.3	58.2
	High Ti	0.01	21.2	3.16	23.7	49.4	0.67	0.91	0.08	0.44	99.7	58.7	34.4
A-880761 (Gra-B)	*LowTi*	0.01	7.18	7.48	45.4	37.2	0.58	0.87	0.06	0.90	99.7	19.5	64.7
	High Ti	0.02	19.8	3.48	26.0	47.8	0.68	0.86	0.02	0.54	99.2	54.7	37.8
A-881388 (Gra-B)	*LowTi*	0.00	7.11	7.07	45.3	37.8	0.61	0.72	0.04	0.95	99.6	19.5	65.3
	High Ti	0.02	19.1	3.47	25.5	49.4	0.68	0.91	0.08	0.56	99.8	54.2	38.1
Agoult (Gra-B)	*LowTi*	0.02	6.57	6.78	45.3	38.2	0.61	0.85	0.11	0.87	99.3	18.4	66.7
	High Ti	0.02	21.8	2.96	22.8	50.0	0.68	0.75	0.10	0.50	99.7	60.4	33.2
A-87272 (Type 7)	*LowTi*	0.04	2.13	8.75	51.3	34.2	0.60	0.46	0.15	0.94	98.6	5.9	75.0
	High Ti	0.06	22.1	2.33	23.0	49.9	0.81	0.41	0.12	0.48	99.2	61.4	33.5
DaG 945 (Type 4)	*LowTi*	0.02	7.74	7.39	42.5	39.1	0.64	0.73	0.08	0.92	99.0	21.6	62.3
	High Ti	0.01	20.9	3.31	24.7	49.3	0.68	0.90	0.06	0.53	100.3	57.3	35.6
NWA 2362 (Type 5)	*av (n=16)*	0.13	1.99	8.79	52.5	33.7	0.68	0.40	0.08	0.71	99.0	5.5	75.7

Table 3. Bullk chemical compositions (oxide in wt% and others in ppm).

	A-881467	A-880702	A-881388	A-880761	Agoult	
Split	52	31	64	42	A	B
Lab	*TMU*	*TMU*	*TMU*	*TMU*	*LGCA*	*IUEM*
SiO_2	48.0	48.1	48.6	48.6		
TiO_2	0.76	0.682	0.702	0.616	0.62	0.68
Al_2O_3	11.7	12.8	12.1	12.8	13.14	13.23
Cr_2O_3	0.317	0.311	0.306	0.302		0.36
FeO	20.9	20.2	20.1	19.2	17.84	21.16
MnO	0.54	0.519	0.519	0.513	0.56	0.64
MgO	7.1	7.48	6.40	7.50	7.77	7.20
CaO	10.7	10.4	11.5	10.6	11.40	11.03
Na_2O	0.532	0.508	0.495	0.474		0.41
K_2O	<0.006	0.050	0.025	0.040		0.04
P_2O_5						0.074
Li						8.83
Be						0.21
Sc	34.7	32.6	32.6	30.8		30.38
V	69	77.4	77.2	64.2		74.98
Co	6.1	4.15	6.32	4.62	8.74	6.00
Ni					(5)	1.01
Cu						0.88
Zn						0.97
Ga		3.36	3.96	2.96	(2.01)	1.52
Rb					0.18	0.10
Sr		91.3	82.6	77.5	87.2	74.72
Y	16.3	18.3	16.3	15.6	17.24	14.50
Zr		47.8	51.7	52.7	40.10	36.45
Nb					3.83	3.41
Cs					0.010	0.004
Ba					30.3	25.60
La	2.50	2.67	2.28	2.44	2.21	1.81
Ce	6.3	6.72	5.78	6.06	5.81	4.71
Pr	1.01	1.03	0.886	0.918	0.890	0.715
Nd	5.03	5.04	4.36	4.47	4.39	3.70
Sm	1.71	1.72	1.55	1.54	1.48	1.27
Eu	0.65	0.627	0.557	0.571	0.602	0.561
Gd	2.25	2.17	1.93	1.93	2.03	1.68
Tb	0.44	0.404	0.365	0.364	0.384	0.326
Dy	3.00	2.70	2.43	2.43	2.62	2.31
Ho	0.68	0.59	0.53	0.53	0.575	0.519
Er	1.96	1.73	1.55	1.56	1.69	1.57
Tm	0.292	0.26	0.23	0.23		
Yb	1.95	1.69	1.50	1.52	1.63	1.57
Lu	0.298	0.258	0.229	0.232	0.255	0.231
Hf	1.6	1.15	1.35	0.908	1.03	1.01
Ta		0.034	0.300	0.274	0.190	0.18
W					0.020	0.030
Pb					1.46	0.13
Th	0.273	0.305	0.266	0.293	0.261	0.209
U	0.038	0.067	0.091	0.080	0.074	0.070

(Continued)

Split	A-87272 ,140 *TMU*	A-87272 ,26 *TMU*	A-87272 ,25 *IUEM*	DaG 945 A *TMU*	DaG 945 A *IUEM*	NWA 2362 A *TMU*	NWA 2362 A *IUEM*
SiO_2	49.1	47.9		50.8		50.9	
TiO_2	0.51	0.475	0.51	0.617	0.65	0.484	0.51
Al_2O_3	12.9	13.4	13.70	11.8	-	12.3	13.68
Cr_2O_3	0.325	0.315	0.30	0.322	0.32	0.326	0.32
FeO	20.2	20.0	19.36	20.2	20.07	20.0	20.07
MnO	0.59	0.563	0.59	0.569	0.60	0.565	0.63
MgO	7.2	7.37	7.08	6.59	7.40	7.32	7.60
CaO	9.8	10.7	10.36	9.34	10.80	9.96	11.02
Na_2O	0.401	0.395	0.38	0.441	0.46	0.374	0.39
K_2O		0.0277	0.04	0.0372	0.06	0.0321	0.04
P_2O_5			0.08		0.065		0.070
Li					9.62		7.41
Be			0.23		0.24		0.19
Sc	29.5	30.0	29.4	31.8	31.09	31.8	30.92
V	69	71.8	70.13	60.7	58.88	67.9	66.54
Co	5.8	4.88	4.53	4.62	3.69	4.22	3.99
Ni			<1		0.47		2.44
Cu			0.20		0.57		0.87
Zn			0.30		0.35		2.23
Ga			1.47		1.30		1.37
Rb			0.15		0.12		0.13
Sr		72.2	80.76	72.6	72.29	87.9	85.1
Y	10.2	14.9	13.94	8.91	11.97	12.4	12.21
Zr		35.3	23.84	41.7	42.26	24.7	26.90
Nb			2.89		3.26		1.93
Cs			0.005		0.00		0.003
Ba			25.90		27.68		29.00
La	1.55	2.07	2.06	1.03	1.10	1.42	1.31
Ce	4.28		5.08		2.71		3.45
Pr	0.576		0.771		0.40		0.54
Nd	2.87		3.99		1.99		2.86
Sm	0.95	1.38	1.30	0.799	0.77	1.09	1.05
Eu	0.59	0.636	0.578	0.599	0.58	0.544	0.532
Gd	1.30		1.85		1.09		1.47
Tb	0.259		0.344		0.2		0.277
Dy	1.85		2.30		1.78		1.91
Ho	0.42		0.509		0.41		0.433
Er	1.28		1.49		1.30		1.28
Tm	0.196						
Yb	1.34	1.58	1.40	1.29	1.45	1.29	1.28
Lu	0.204	0.245	0.207	0.223	0.22	0.203	0.194
Hf	0.68	0.929	0.69	1.00	1.14	0.908	0.82
Ta			0.167		0.19		0.106
W			0.044		0.05		0.025
Pb			0.11		0.13		0.06
Th	0.201		0.242		0.29		0.126
U	0.0831		0.082		0.05		0.058

Table 4. Oxygen isotope results

SAMPLE	N	$\delta^{17}O‰$	1σ	$\delta^{18}O‰$	1σ	$\Delta^{17}O‰$	1σ
A-87272	2	1.819	0.046	3.909	0.074	-0.230	0.007
A-880761	2	1.717	0.054	3.692	0.106	-0.218	0.002
A-880761 (EATG residue)	1	1.633		3.593		-0.250	
A-880702	2	1.656	0.027	3.636	0.052	-0.250	0.001
A-881388	3	1.668	0.039	3.636	0.086	-0.238	0.009
A-881467	3	1.713	0.064	3.686	0.124	-0.219	0.010
A-881467 (EATG residue)	1	1.648		3.622		-0.250	
Agoult	6	1.664	0.019	3.630	0.031	-0.239	0.017
NWA 2362	2	1.668	0.058	3.663	0.113	-0.252	0.001
DAG 945	2	1.747	0.017	3.786	0.036	-0.237	0.002

Figure Captions

Fig. 1. Photomicrographs of granulitic eucrites. A-880802 (a) and -881467 (b) (type A) show heterogeneous granulitic textures, whereas A-880761 (c), A-881388 (d), and Agoult (e, f) (type B) (b) have granulitic textures with more sorted-grain sizes of minerals. Agoult has a remnant subophitic textures consisting of anhedral pyroxene and elongated plagioclase. (a)-(f) Plane light; (f) crossed-polarized light.

Fig. 2. Photomicrographs of A-87272 (type 7) (a), DaG 945 (type 4) (b), and NWA 2362 (type 5) (c). A-87272 and DaG 945 have coarse-grained textures. NWA 2362 shows a medium-grained granular texture. Plane light.

Fig. 3. Combined X-ray maps (Mg, Ca, and Al Kα). In type A granulitic eucrites, A-87272 (type 7), and DaG 945 (type 4), there are remnant Ca-zoning toward portions rich in silica minerals (relict mesostasis). In type B granulitic eucrites, pyroxenes are grains of low-Ca pyroxene and augite. There are local concentrations of silica minerals and augite which are relict mesostasis. NWA2367 (type 5) does not have remnant Ca zoning. Low-Ca pyroxenes: red; high-Ca pyroxene: yellow; plagioclase: light blue; silica minerals: blue; oxide minerals: green.

Fig. 4. Pyroxene compositions. Pyroxenes are low-Ca pyroxene and augite with homogenous Mg/Fe ratios. The intermediate Wo contents are due to incomplete resolutions of electron microprobe.

Fig. 5. Plagioclase compositions. Type B granulitic eucrites and DaG 945 shows wide ranges of the plagioclase compositions whereas type A granulitic eucrites and A-87272 show limited compositions.

Fig. 6. Spinel compositions. Except for NWA 2362, all eucrites studied here show compositional variations toward ulvöspinel.

Fig. 7. CI-normalized REE compositions of eucrites studied here and EET 90020. The

reference chondrite is from Evensen et al. (1978).

Fig. 8. Juvinas-normalized patterns of residual eucrites, Agoult, DaG 945, and NWA 2362, and a cumulate eucrite, Moore County.

Fig. 9. Oxygen three isotope plot showing the composition of the metamorphosed eucrites examined in this study in relation to the HED, angrite and main group (M-G) pallasite data of Greenwood et al (2005, 2006) (Howardites and polymict eucrites have not been plotted). Open red circles represent EATG residues. TFL: Terrestrial Fractionation Line, EFL: Eucrite Fractionation Line ($\Delta^{17}O = -0.239 \pm 0.007$ (1σ))

Fig. 10. The effects of oversampling or under sampling of a phosphate phase in a eucrite split. The calculations were made using the Juvinas eucrite (Jv. clast 2, Barrat et al., 2007 and a merrillite found in Sioux County (Hsu and Crozaz, 1996). The patterns of Agoult, DaG 945, and NWA 2362 are shown for comparison.

Fig. 11. The CI-normalized REE patterns of residual eucrites calculated from partial melting with the extraction of partial melts from 0-10 %. Juvinas compositions of a typical eucrite Juvinas (Barrat et al. 2007) are selected for the starting material of the calculations.

Fig. 12. Sc vs La for eucrites studied here and for ranges of Main-Group – Nuevo Laredo trend eucrites, Stannern trend eucrites, and cumulate eucrites.

Fig. 13. Basic time-temperature paths of basaltic eucrites after eruption and solidification. We envision thermal histories (at ~700-1100°C) of eucrites by combination of prolonged burial metamorphism (A) and/or local reheating events (B and C). The local reheating events include magma intrusions (B) and impact events (C). Compared to magma intrusions (2a and 2b), impact events sharply increase the temperatures and in some cases cools rapidly to low temperatures (<800°C) by excavation (3a' and 3b'). In some cases, impact may not cause any significant reheating (3b and 3b'). Prolonged reheating by burial and/or large magma intrusions may cause both pyroxene equilibration (e.g., type 5 and 6) and partial melting (1a

and 1b). Short reheating may cause partial melting but may only cause partial equilibration of pyroxenes (e.g., type 4 and 7) (2a, 3a and 3a'). It is possible that similar reheating events occur but do not exceed the solidus temperatures when the ambient temperatures are lower or the degrees of reheating are smaller (2b, 3b and 3b'). See text.

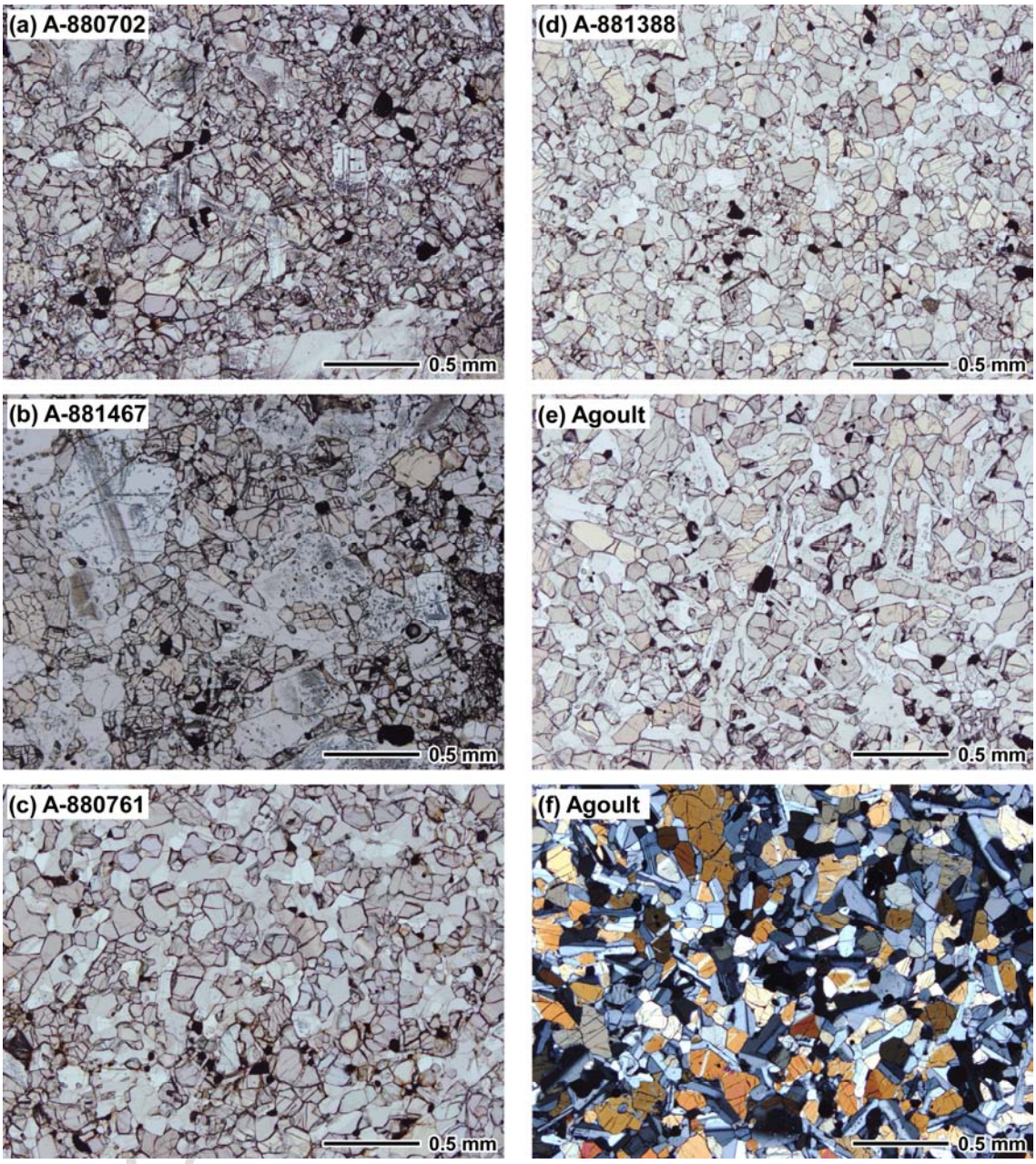

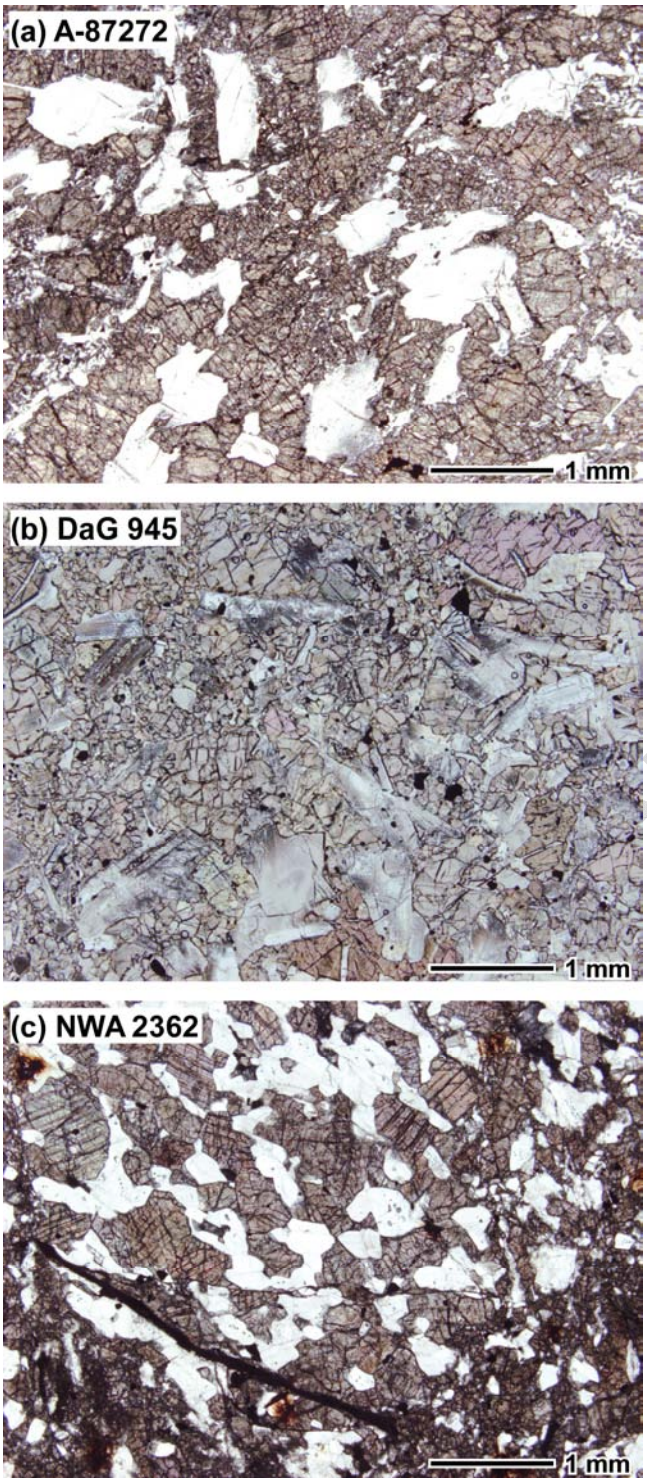

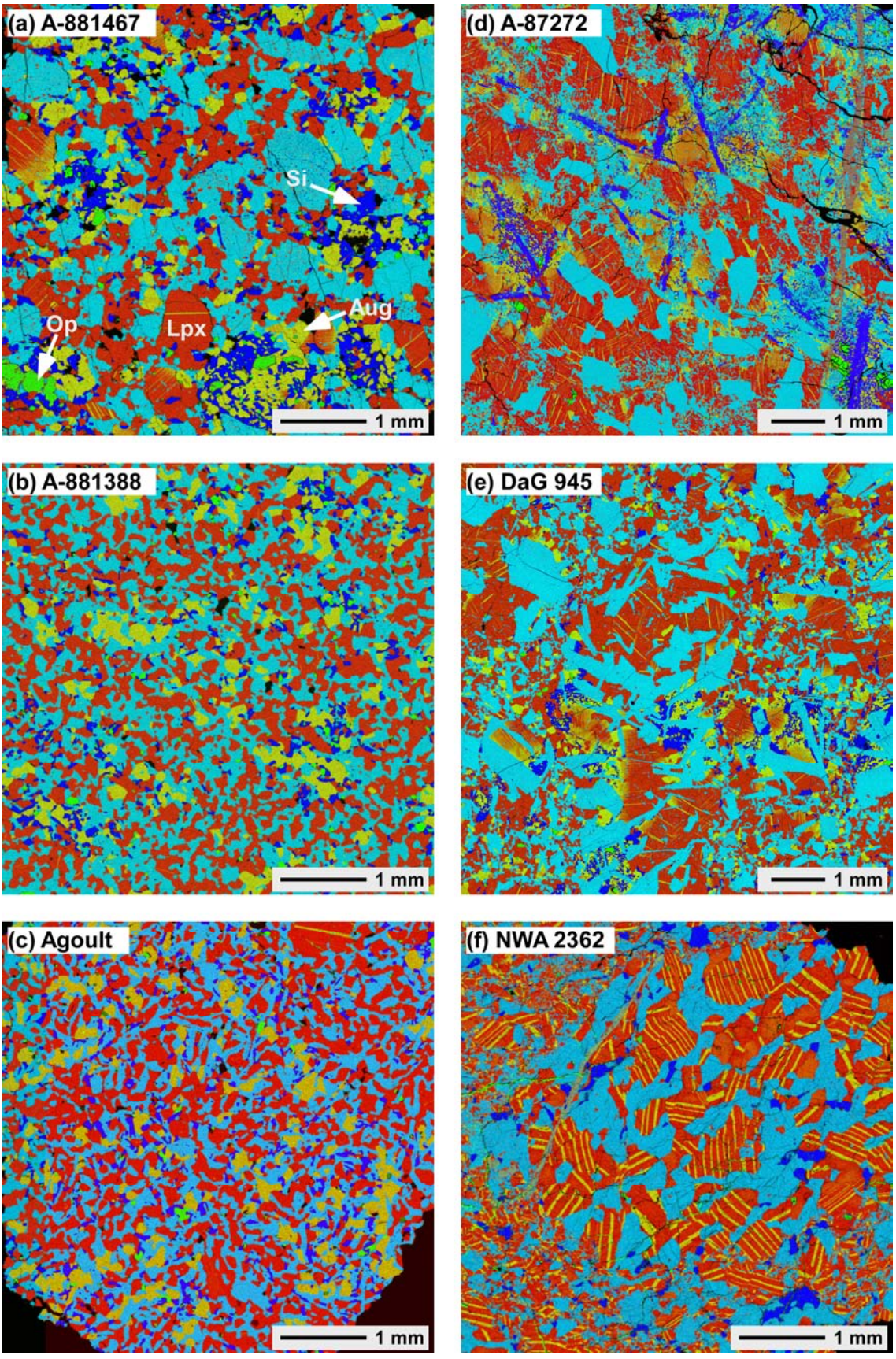
(a) A-881467
Si
Aug
Op
Lpx
1 mm
(d) A-87272
1 mm
(b) A-881388
1 mm
(e) DaG 945
1 mm
(c) Agoult
1 mm
(f) NWA 2362
1 mm

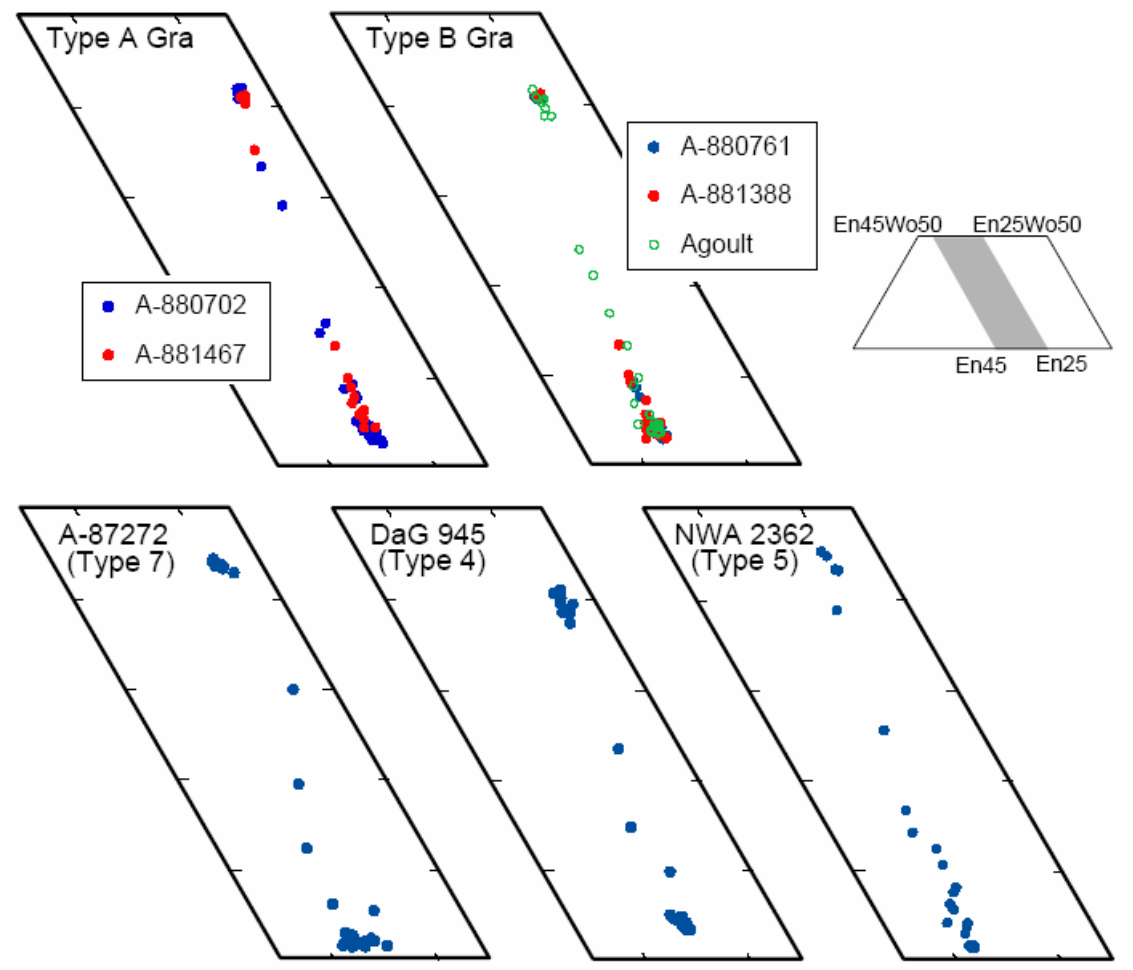

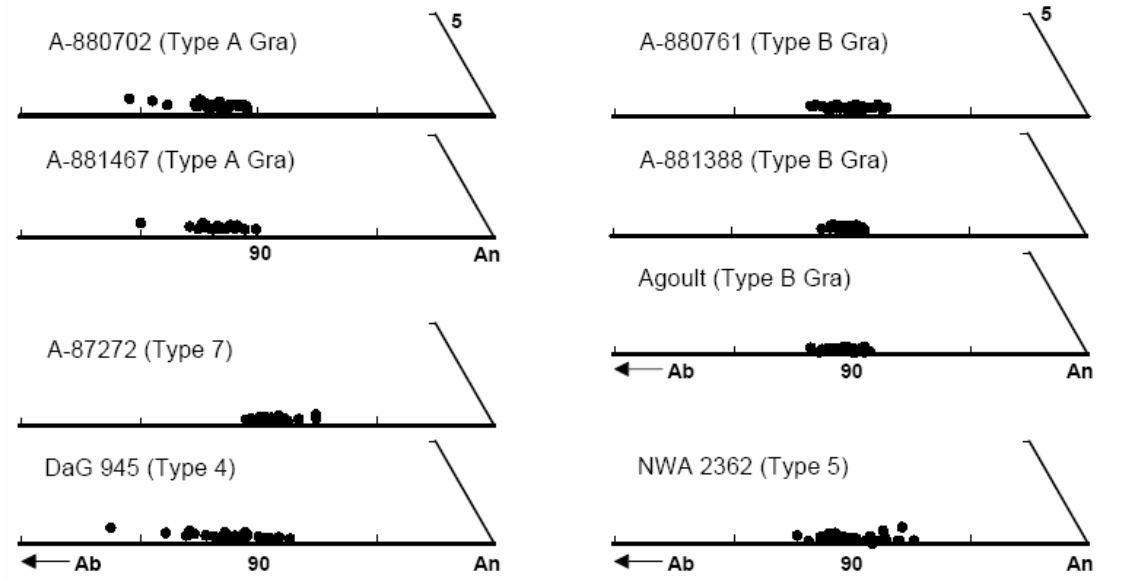

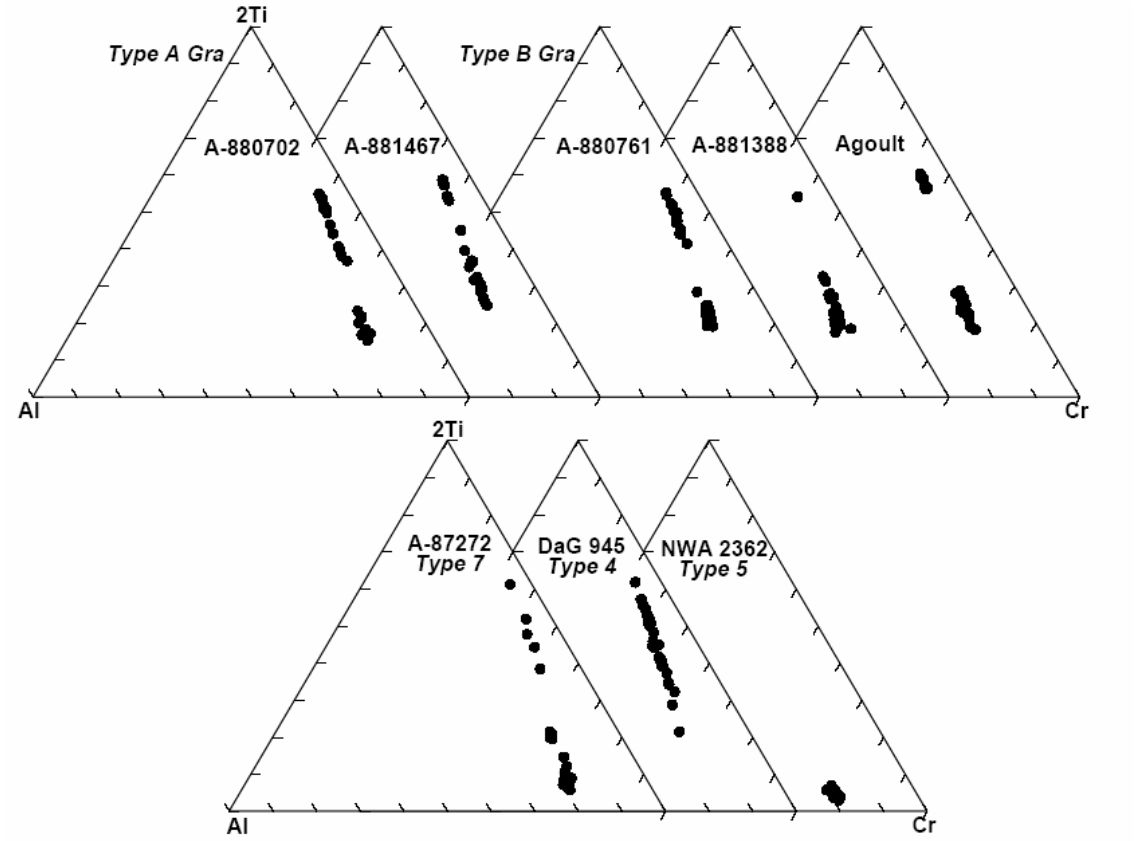

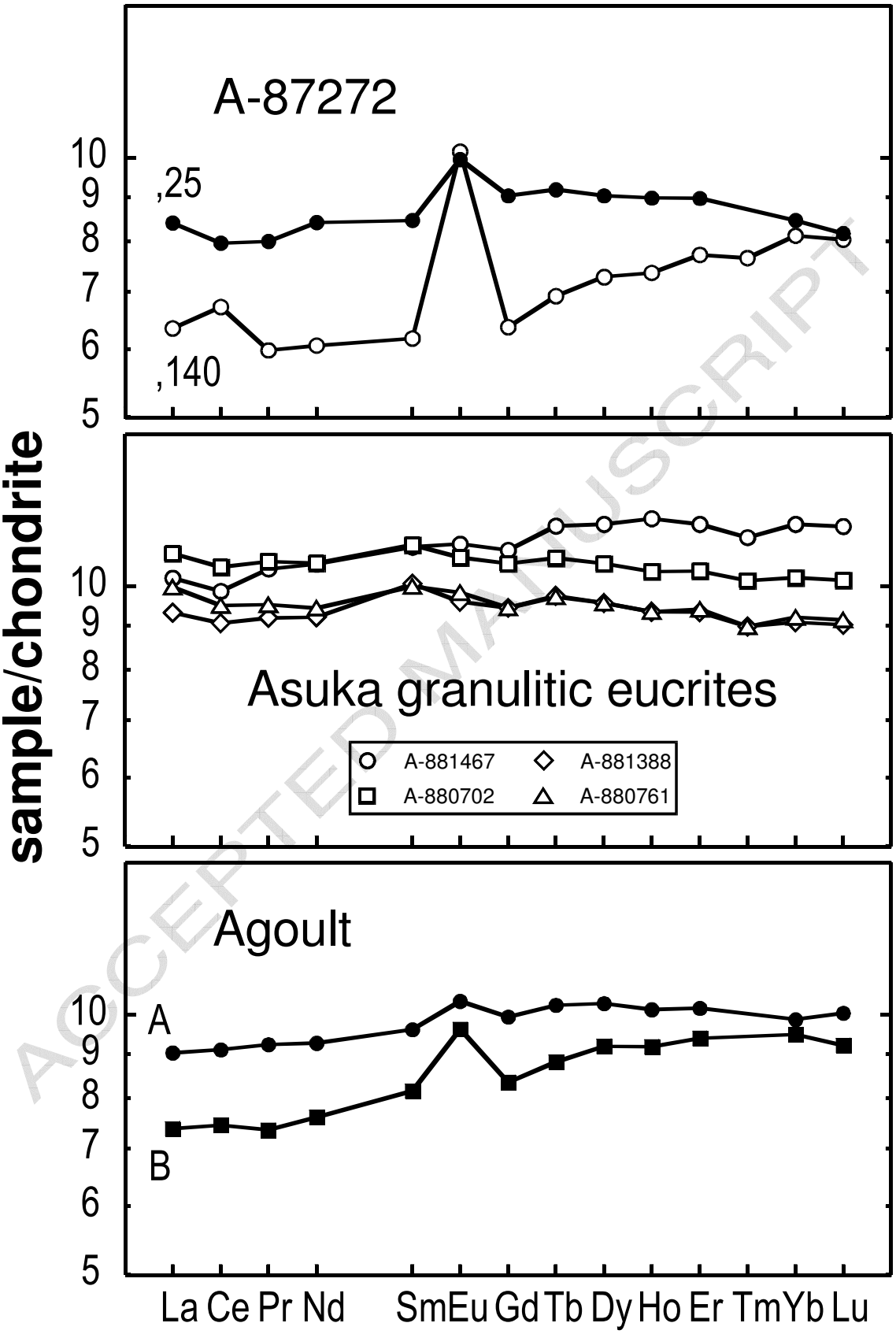

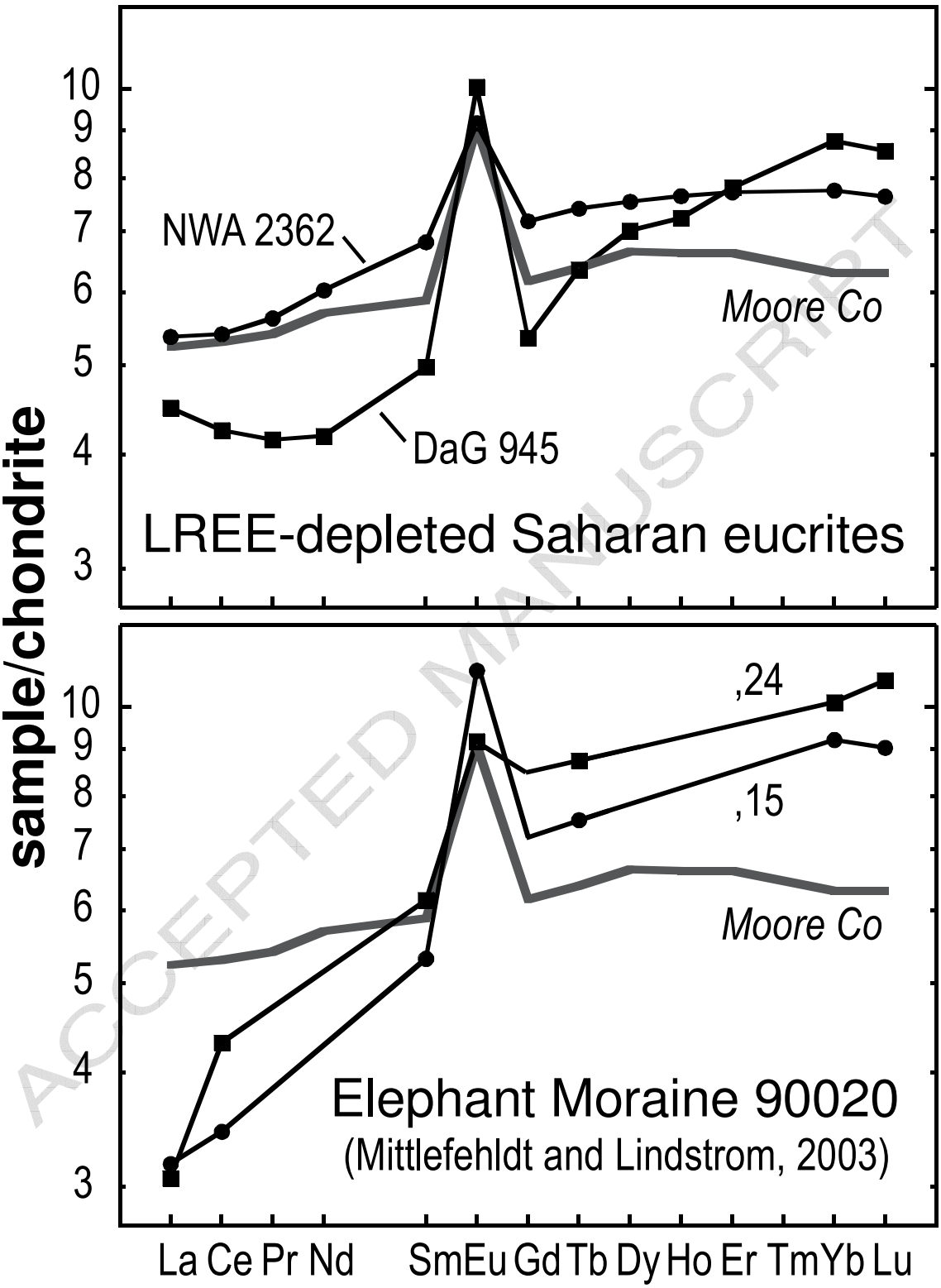

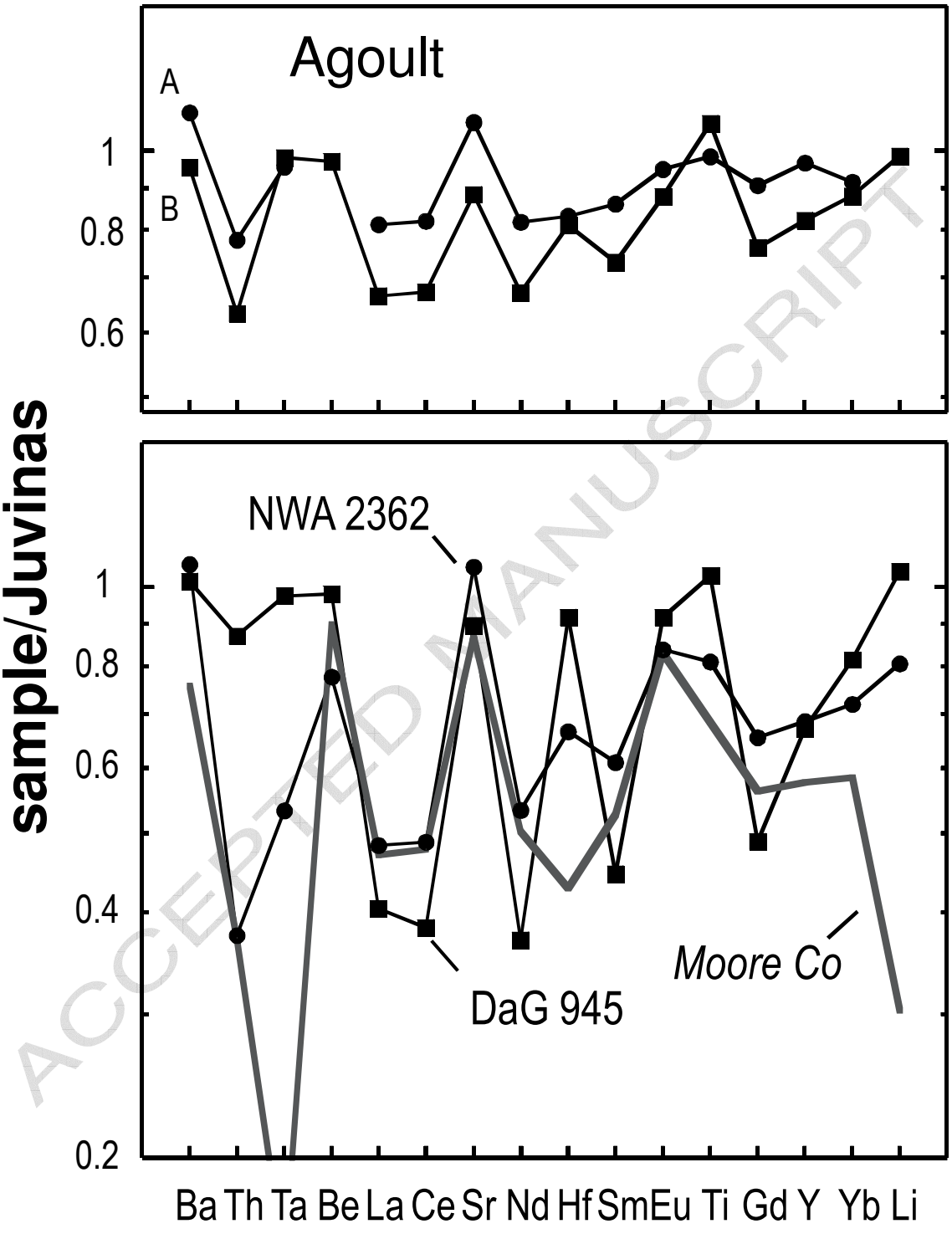

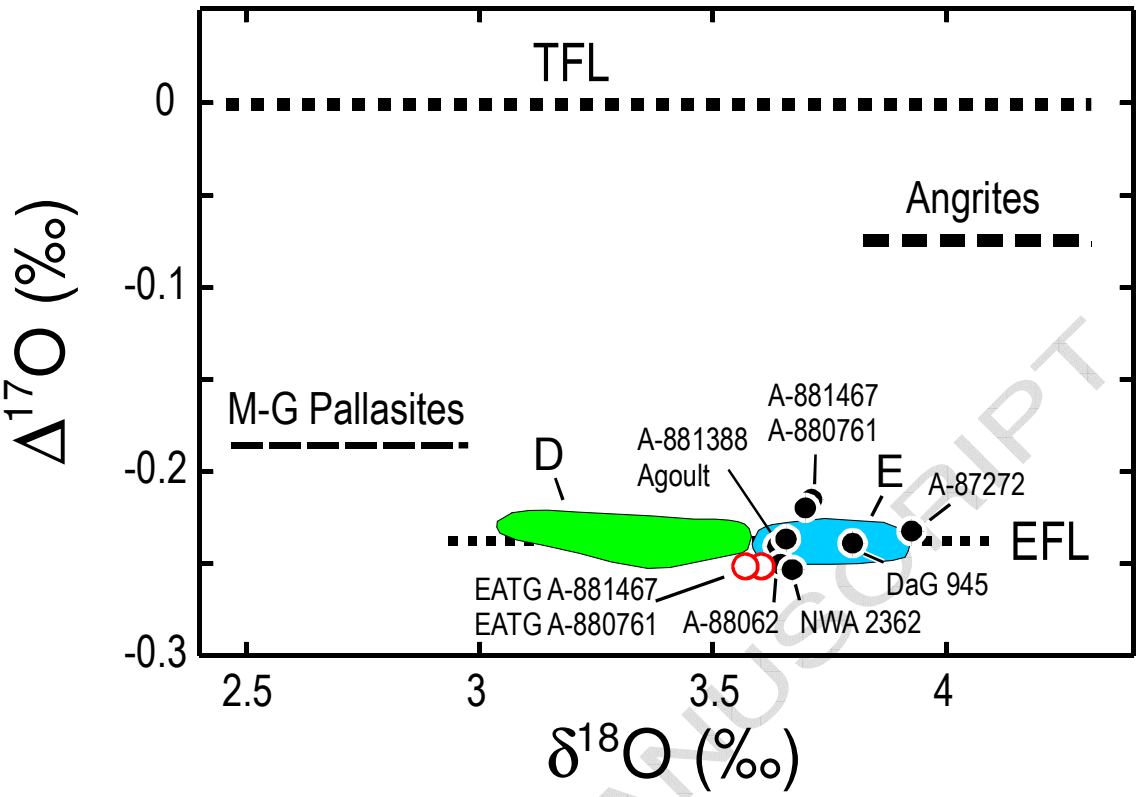

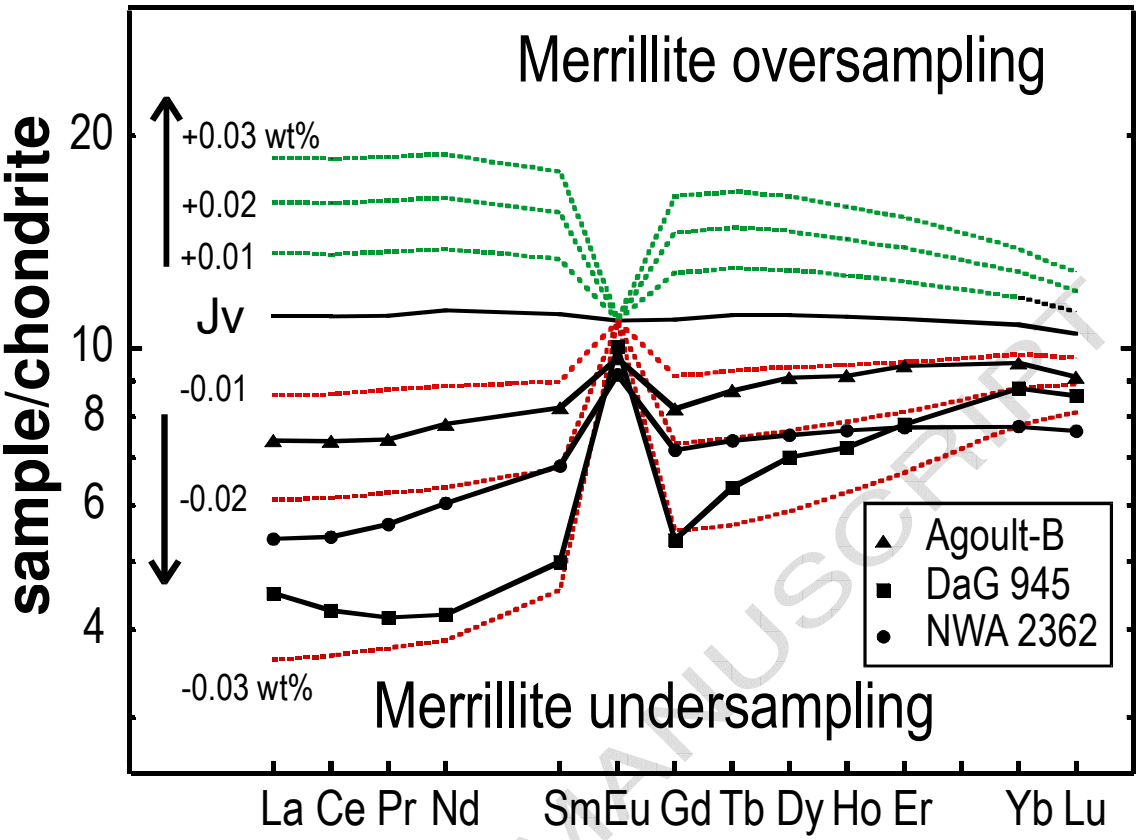

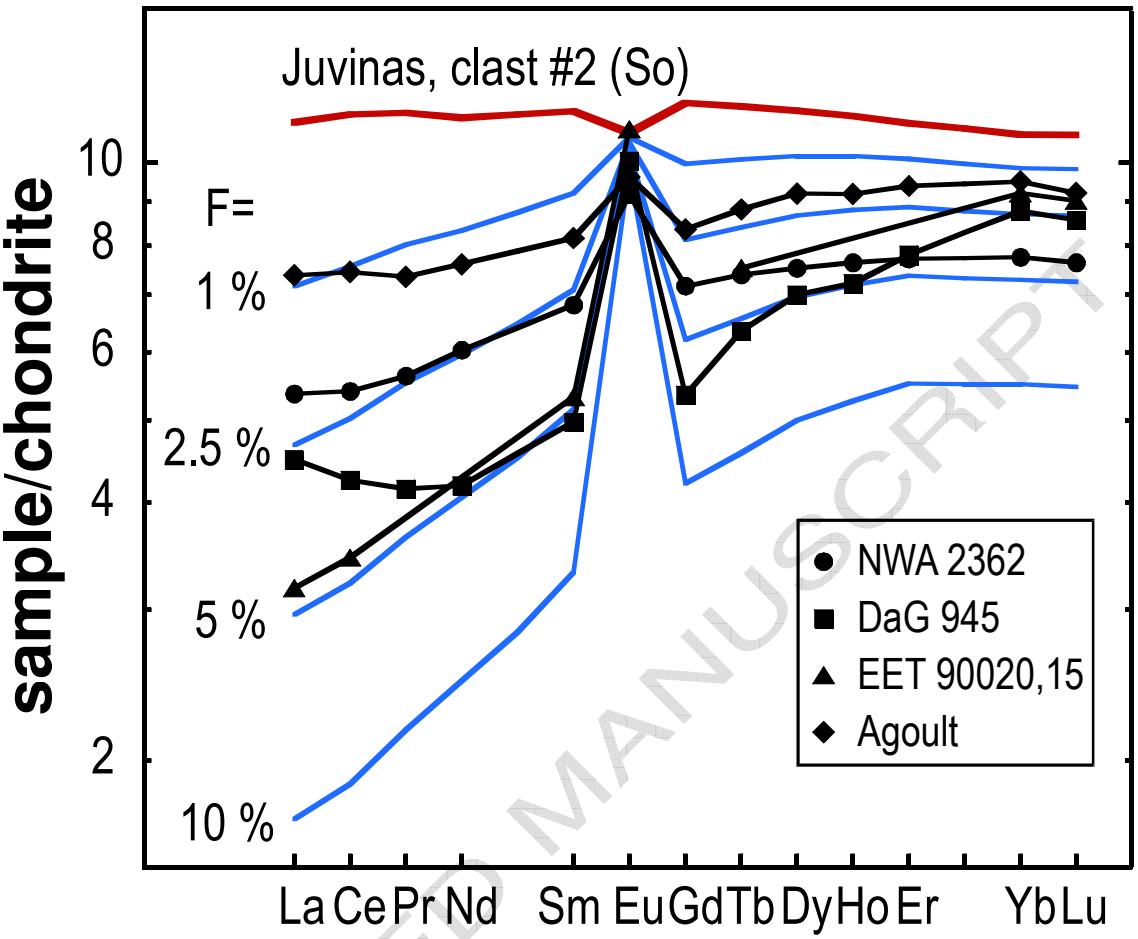

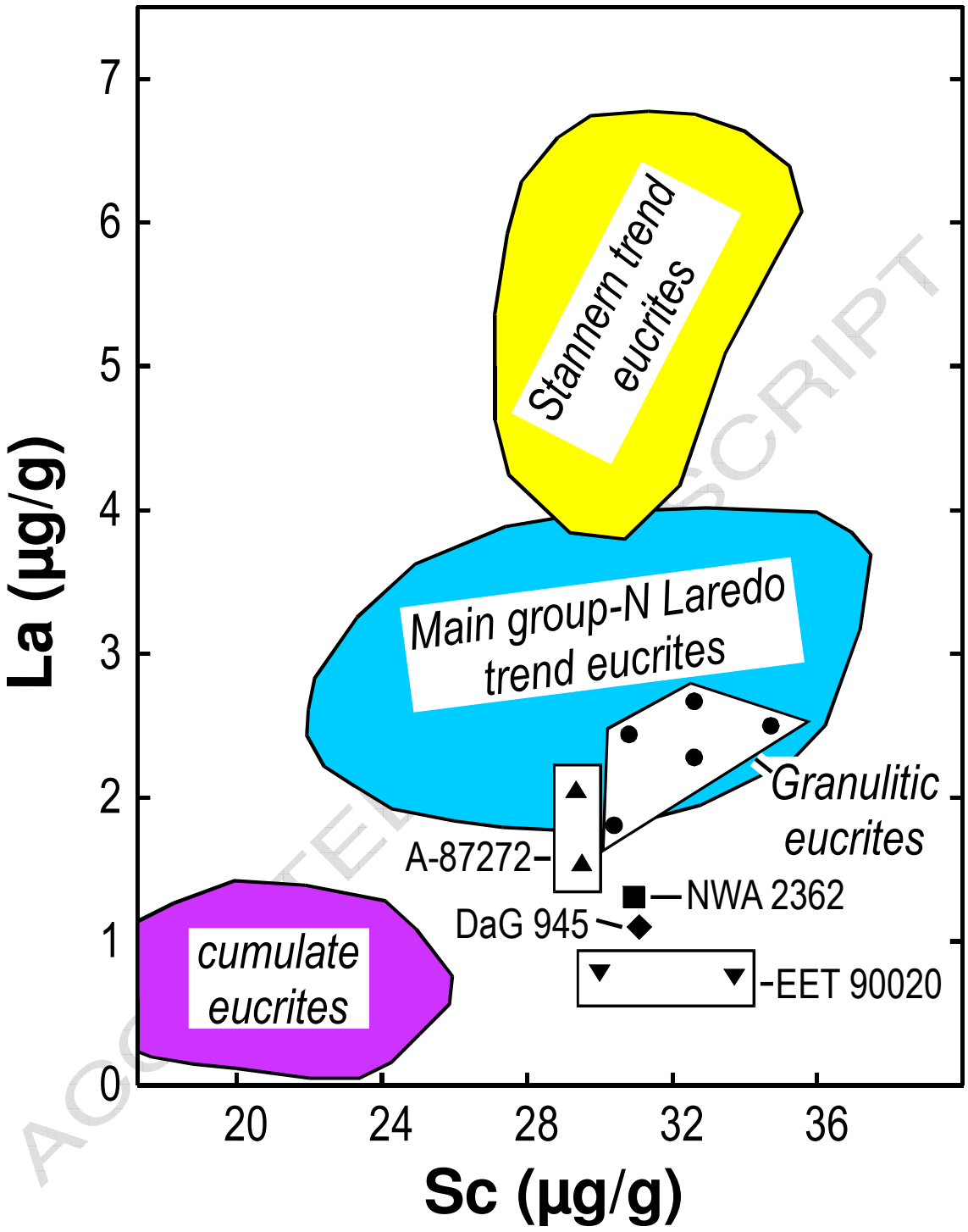
La (µg/g)
Sc (µg/g)
0
1
2
3
4
5
6
7
20
24
28
32
36
Stannern trend eucrites
Main group-N Laredo trend eucrites
Granulitic eucrites
A-87272
NWA 2362
DaG 945
EET 90020
cumulate eucrites

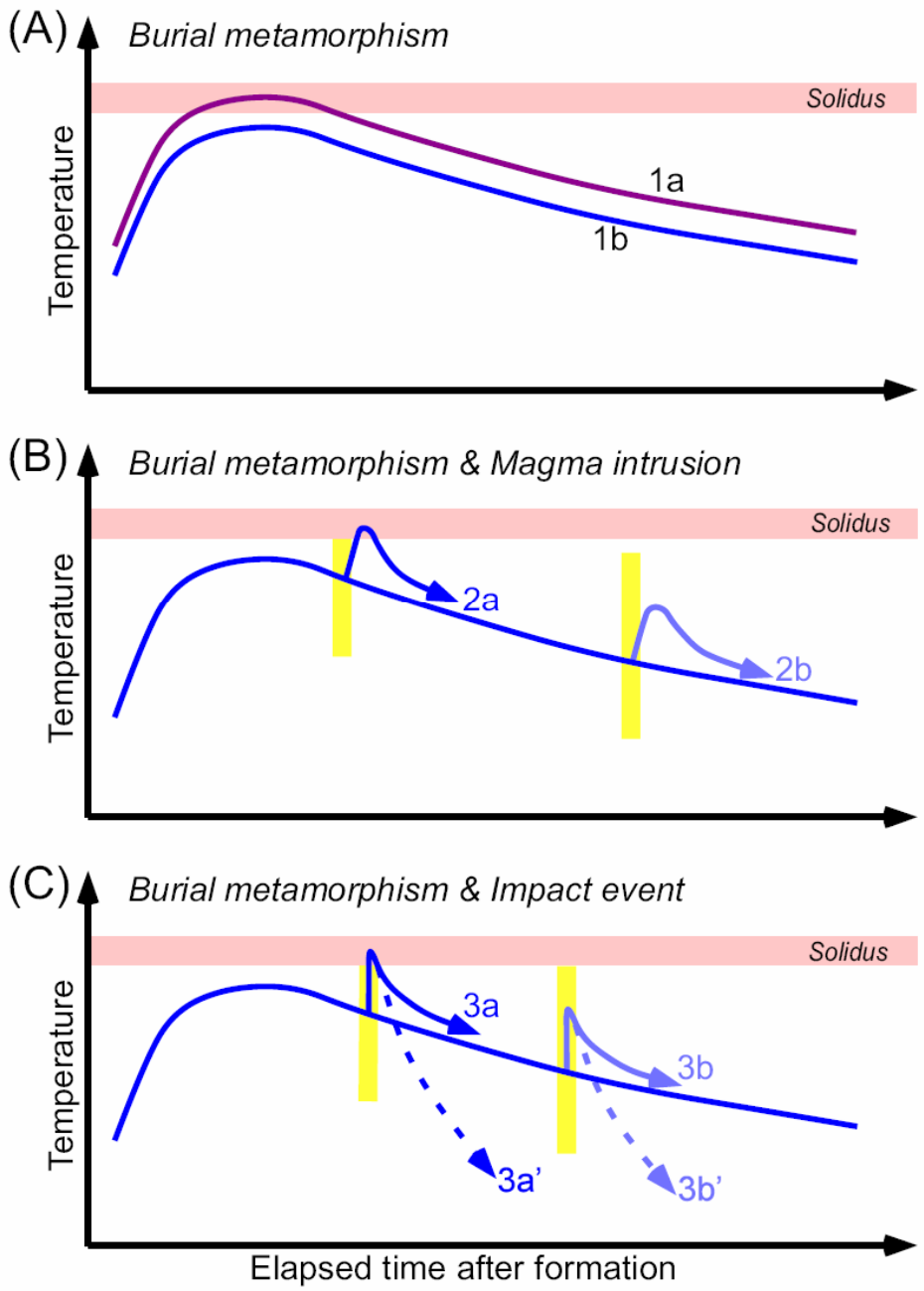
(A)
Burial metamorphism
Solidus
Temperature
1a
1b
(B)
Burial metamorphism & Magma intrusion
Solidus
Temperature
2a
2b
(C)
Burial metamorphism & Impact event
Solidus
Temperature
3a
3b
3a'
3b'
Elapsed time after formation